PRELIMINARY DESIGN OF THE WIYN 3.5 METER TELESCOPE

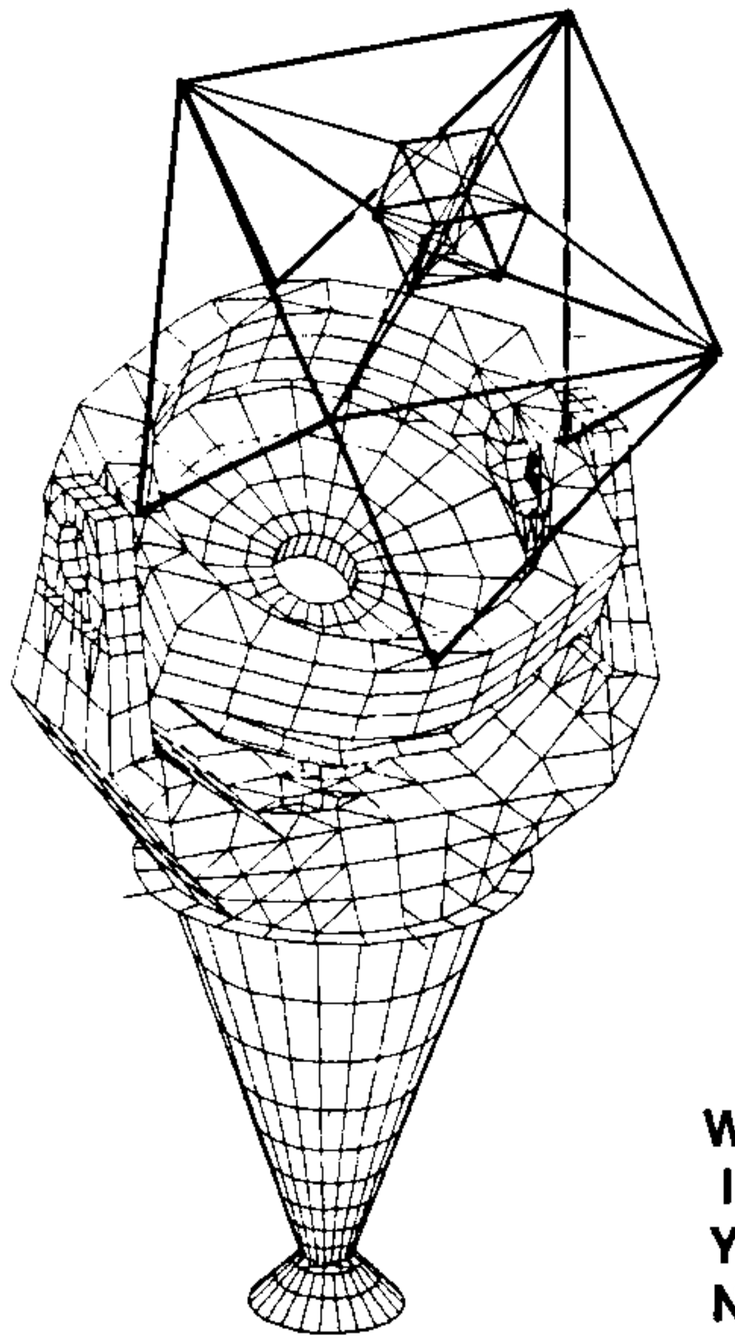

Wisconsin
Indiana
Yale
NOAO

for

NATIONAL OPTICAL ASTRONOMY OBSERVATORIES

P. O. Box 26732
950 N. Cherry Ave.
Tucson, Arizona 85726-6732

by

L & F INDUSTRIES

P. O. Box 40
2110 Belgrave Ave.
Huntington Park, Ca. 90255

No. WODC 02-07-01 - June 1991

INDEX

1.0 INTRODUCTION

This report summarizes the current preliminary design of the Wisconsin-Indiana-Yale-NOAO (WIYN) 3.5 Meter Telescope, including recent analysis and design performed for NOAO by L & F Industries. The purpose of the recent work has been to optimize critical structural features, determine magnitude and phase response of the structure to support control system analysis and design, and to further define the telescope mechanical systems.

To these ends, considerable finite element analysis has been performed on the Optics Support Structure to passively align the optics as the OSS rotates through the gravity field, and on the entire telescope to predict wind effects and modal performance for the optimized structure.

Additional engineering data and current layout drawings are included in the appendix. Reference is hereby made to the earlier report, "Engineering Report - Preliminary Design Study - WIYN 3.5 Meter Telescope" dated June, 1990. Some portions of the 1990 report are still current, and have been included in this report.

2.0 STRUCTURAL AND MECHANICAL CONFIGURATION

2.1 SYSTEM DESCRIPTION

The WIYN 3.5 Meter Telescope design summarized herein consists of an Alt-Azimuth Fork mount, using rolling element bearings to define the altitude axis and lower end of the azimuth axis. The upper end of the azimuth axis is defined using drive and idler rollers which are in turn supported by rolling element bearings. The system is shown on drawings D305003, E305007 sheet 2, E305008, E305009, E305020, E305030, D305031, and D305032 as well as graphics plots in Figures 1 through 26. The 3.5 meter f1.75 primary mirror and f6.3 secondary mirror focus at either of two Nasmyth instrument locations, at modified Cassegrain, or at a fourth folded Cassegrain instrument location, on the OSS center section.

The two main rotating structural assemblies of the mount are the Optics Support Structure and the Fork.

The OSS Assembly (E305009) consists of three major subassemblies:

1.) The mirror cell assembly includes the cell structure (ref KPNO Drawing 3500.0002073E, not included in this report), the primary mirror, and its

support and ventilation systems.

2.) The center section includes the center section structure, mirror cover, altitude bearings, and (2) counterweight assemblies. It also supports the altitude drive disks and primary truss.

3.) The secondary end includes the secondary main truss, square frame, vanes, secondary center structure, and secondary mirror, cell, and support system.

The Fork Assembly (E305030 and E305007 sheet 2) consists of the cone, azimuth drive disk, fork weldment, pillow blocks, altitude axles, and Nasmyth instrument rotators.

In addition there is a stationary lower bearing support pedestal (D305003) and square frame azimuth support system (E305008), used to define the telescope to ground.

2.2 STRUCTURAL DESIGN

The structural design is intended to maximize stiffness and reduce weight, achieving relatively high modal performance without the necessity of hydrostatic bearings. High stiffness and low weight effect small deflections due to gravity and wind loading, and high structural resonant frequencies. In addition, the low weight may result in cost savings, but will certainly improve thermal response of the structure to ambient temperature changes. This will then have a beneficial effect on seeing and optical alignment.

As can be seen on the drawings and graphics plots herein, the telescope structure is generally constructed using plate fabrications. Plates used are predominantly 3/8" and 1/2" thick carbon steel. Notable exceptions to this are the secondary and primary end main truss members, which are made from steel tubing. All weldments will be thermally stress relieved, and low hysteresis bolted joints will be used where mechanical disassembly is desirable. Detailed descriptions of plate thicknesses and member sizes are included in the graphics plots, Figures 4 through 12.

2.3 BEARINGS

Consideration of various rolling element bearing types was made during the 1990 preliminary design study for both the altitude and azimuth axes. A detailed discussion of all configurations investigated is beyond the scope of this report. However, a description of the current favored types, and reasons for these selections, is provided as follows:

2.3.1 Altitude Bearings

The moment-carrying duplex pair of angular contact ball bearings, shown on E305007 sheet 2, is preferred for the altitude bearings. The bearings tentatively selected are Kaydon KG250AR(tbd)BR2Z, selected to .0008 in. runout. Each duplex pair would be preloaded sufficient to keep all clearance out of the bearing under full load of the OSS assembly. The bearing support axles will be pre-cocked to accomplish a nominally zero moment on each pair with the system fully assembled and under the influence of gravity. While these bearings may not have friction as low as spherical roller radial bearings, they are likely to have lower non-repeatable runout due to the use of more precise balls (rather than individually machined rollers). The friction can be minimized by using a low preload and by precocking the axles. The bearings have good availability and relatively low cost.

2.3.2 Azimuth Bearings

The upper end of the azimuth axis will be defined by two drive and two idler roller units, spaced at 90° around the axis. The bearings used to support these rollers, and the rollers themselves will be manufactured to minimize non-repeatable pointing errors.

The lower azimuth bearing is a spherical roller thrust bearing, either SKF 29292 or FAG 29292E.MB. This bearing provides the self-alignment feature necessary for this application, has low friction, and is available at reasonable cost. A test of non-repeatable runout (or "noise") on the similar bearing used at Apache Point Observatory has been conducted and has shown this bearing type to be acceptable (ref WODC 02-06-01). The bearing and an earlier-considered alternate concept for a self-aligning ball bearing, are shown on D305003.

2.4 DRIVES

Friction drives are planned for both telescope axes. The altitude axis will use one drive unit near the inside of each fork tine, with the drive mounted to the fork and driving against an altitude drive disk mounted to either edge of the center section of the OSS (ref E305009).

The azimuth axis drive concept uses two drives at 180° to each other driving against a drive disk at the top of the cone of the fork. This arrangement is shown on drawing E305008. One quadrant of the upper azimuth support system including one drive assembly is shown at an enlarged scale on drawing E305008. In the case of both drives (altitude and azimuth) the drive boxes have stiff restraints only in the tangential (drive)

direction. They are otherwise free to articulate except that they are guided by rollers registering against the edges of the drive disks which are perpendicular to the drive surface, and the dual preloaded-roller feature prevents rotation of the unit about an axis parallel to the rotation axis. A similar arrangement is used on the Apache Point Observatory (APO) 3.5 Meter Telescope.

Direct friction drives similar to those developed for the Magellan Project[1] have been chosen for the WIYN telescope. A layout is shown on drawing D305031. This design consists of a 4 in. diameter traction drive roller directly connected to the frameless drive motor. The drive disk/drive roller diameters provide 30:1 and 35:1 reduction ratios to the altitude and azimuth axes, respectively. Inland model QT-7801 motors have been selected for the telescope drives. Testing of the Magellan prototype, and controls analysis for the WIYN system based upon scaled properties, indicate that the drives will provide excellent control of the telescope[3,4].

2.5 ENCODERS

Incremental and absolute encoders will be used to determine the telescope position.

The azimuth axis will use two ROD 800 series incremental encoders friction coupled to the azimuth drive disk. They will be mounted to the upper azimuth support square frame at 180° to each other and oriented to the pier in such a way as to minimize error due to varying strain in the pier. A Sony Magnaswitch will be used for absolute position encoding. The model and quantity of fiducial points are to be determined.

The altitude axis will use (one or two) ROD 800 series incremental encoders friction coupled to one or both altitude drive disks. They will be mounted to the fork tine and therefore determine the altitude position of the OSS with respect to the fork. A Sony Magnaswitch will be used for absolute position encoding. The model and quantity of fiducial points for the altitude axis are also to be determined.

The resolution stability of both encoder types is believed to be adequate over the anticipated operating temperature range.

2.6 INSTRUMENT ROTATOR

The Nasmyth Instrument Rotators are integrated into the pillow block assemblies. Drawing E305020 shows the layout of the major components of each rotator.

2.6.1 General description

The Nasmyth Instrument Rotator consists of a rotating turntable mounted on the pillow block with its axis of rotation coincident with the telescope optical axis at the Nasmyth focus. Science instruments will attach to a flange that extends beyond the surface of the

fork. A hole through the center of the turntable provides clearance for the 1° FOV beam plus allowance for mounting a field corrector.

The turntable is rotated by a single DC motor and friction drive rolling on the perimeter of the disk. The rotator position is encoded by an incremental encoder friction coupled to the drive surface. Absolute position is referenced to an electronically readable position sensor that provides a fiducial position at one rotation angle.

A caliper, disk type, failsafe brake is used to prevent rotator motion when the motor drive is off. The braking force is applied by springs and pneumatically released. A locking pin will also be provided at the rotator stow position to prevent rotation during instrument changes. Hard stops and limit switches will restrict rotation to +/-180°.

Identical rotators will be provided at both Nasmyth positions. A mechanically similar rotator is being used successfully on the APO 3.5 meter telescope.

2.6.2 Mechanical

A 25 inch bore, duplex pair of angular contact ball bearings is used to support the Nasmyth instrument and react its cantilever moment. The selection was based upon physical size needed to clear the light beam and resulted in a bearing oversized for the load it has to carry:

	Dynamic capacity (pounds)	Calculated load (pounds)
Radial load:	14,100	2,664
Axial load:	40,700	1,658

The bearing jitter goal is 0.0005 inch maximum. Bearing manufacturers do not seem to have much data on non-repeatable runout. They do believe that this will be about 0.0005 inch due to the balls alone. Deformation of the balls and races under load should reduce this runout. The bearing jitter should, therefore, be less than the 0.0005 inch but we cannot be absolutely sure of this.

The concentricity goal of 0.001 inch will be very difficult to achieve and some amount of compensation by the control system may be required. We believe the perpendicularity goal of 10 arcsecs can be met with this design. A fixture to hold the bearing and disk assembly during the finish grinding operation should provide the best concentricity and perpendicularity achievable.

The proposed design will be able to accelerate and slew a full instrument load at the required 1°/sec^2 and 5°/sec rates respectively. Tracking control will be provided by the control system. It is believed that the goal of +/-5 arcsec (rotator) positioning accuracy can be achieved with relative ease.

2.7 MISCELLANEOUS MECHANICAL SYSTEMS

2.7.1 Primary mirror cover

A biparting bellows type mirror cover is planned, the concept for which is indicated on E305030 and E305009. While a formal preliminary design has not yet been developed for this subsystem, the concept anticipated is described below:

Each biparting half of the cover consists of four slender rectangular panels made from approximately 1" thick aluminum honeycomb. The panels are connected along their long edges with heavy-duty piano hinges oriented in such a way that the assembly can fold to the open position, or extend flat to the closed position. A silicone rubber seal strip will attach on the underside of the cover along each hinge line to preclude dust or dirt from dropping through the hinge and onto the mirror when the cover is closed. A bulbed silicone rubber seal will also attach continuously around the upper inside corner of the center section which the mirror cover will close against.

The cover assembly will be guided along each edge with track rollers running in a channel. The system will be actuated with rotary actuators on alternate hinge axes (or other suitable means), to open and close each biparting half. The cover will be structurally sound, and protect the mirror from blunt impacts of 20 kg-m/sec, as well as meet all of the design requirements set forth in WODC 01-16-01.

2.7.2 Powered counterweights

Two powered counterweight assemblies will be provided, each embedded in a diagonal corner of the center section of the OSS (ref E305009). They serve the purpose of trimming the variable moment around the altitude axis. The total variable moment anticipated at this time amounts to 8,300 in-lbs and is caused by removal of (a portion of) the modified Cassegrain instrument, Tertiary flat swing motion, mirror cover opening, and secondary assembly focus motion. The total trim moment available from the two counterweights will be approximately 11,500 in-lbs. The counterweight design planned for use is a near-duplication of the OSS counterweights used on the Vatican Advanced Technology Telescope (VATT).

2.7.3 Other mechanical systems

Other mechanical devices and systems which will be designed in the detail design phase are: azimuth stow pin and limit switch assemblies, OSS brakes, hard stops, shock absorbers, stay bar, limit switches and stow pin assemblies.

Other devices which will be supplied but which have thus far been designed by NOAO and are therefore not covered in this report are: Tertiary mirror support assembly including base, rotation turntable, tilt mechanism, drive mounts, encoder mounts and limit switch mounts, and secondary and tertiary baffles.

3.0 FINITE ELEMENT ANALYSIS

3.1 INTRODUCTION

The finite element models are shown in the form of graphics plots in Figures 1 through 26. A total of 41 models were created and processed for optimizing and investigative purposes since the earlier work summarized in the June 1990 report. Six models were used to ultimately determine structural performance of the system, summarized in the following pages.

OSS57 is the model of the optics support structure which has been optimized for passive alignment of the optics due to gravity effects. Zenith and horizon gravity loading are applied and combined to determine the optical misalignments due to rotating through the gravity field. This model and its results are described in section 3.5 below.

Models WIYNTZ58 and WIYNTH59 are zenith and horizon-pointing models of the complete telescope to determine wind performance. A simplified primary mirror cell was used with the primary mirror pointing referenced directly from three hard points on the cell. Front and side wind loads were applied, as described later (3.4 Wind Performance).

Models WIYNTM35 and WIYNTM36 are the modal analyses used for subsequent frequency response analysis of the altitude and azimuth axes, respectively. WIYNTM60 is the final fully constrained modal analysis using locked encoder drive stiffness and the optimized OSS and upper azimuth support system. These results are reported in section 3.3, Modal Analysis. Example model sizes are:

WIYNTM60	OSS57
1570 nodes	714 nodes
1964 plate elements	858 plate elements
295 beam elements	183 beam elements
9,228 degrees of freedom	4,266 degrees of freedom
888 bandwidth	486 bandwidth

3.2 OPTICS, INSTRUMENT, AND TELESCOPE WEIGHTS

The following weights were used in, or resulted from, the finite element models:

Subsystems:

Primary Mirror - 4,427 lbs
Axial Support System - 2,856 lbs
Lateral Support System - 278 lbs
Nasmyth Instruments - (2) @ 1,500 lbs
Secondary Assembly - 680 lbs
Tertiary Assembly - 800 lbs
Mirror Cover Assembly - 300 lbs

Totals (including subsystems):

OSS Assembly - 32,810 lbs
5.7E5 lb-sec^2-in (alt axis)
4.4E5 lb-sec^2-in (optical axis)
6.0E5 lb-sec^2-in (perpendicular)

Telescope (rotating) Assembly:
80,000 lbs
1.12E6 lb-sec^2-in (azimuth axis)

3.3 MODAL ANALYSIS

The results of the finite element analyses are presented in Tables 1 through 3 and in the graphics plots in Figures 17 through 22. As can be seen in the left side of Figure 18, the final models were run with the OSS pointing 30° off zenith. It was felt that this was a reasonable compromise between the zenith attitude, where the lateral translation frequency would be slightly lower, and the horizon attitude, where the azimuth rotation frequency would be lower. It is estimated that the lateral translation frequency would be about 2% lower, and the locked encoder azimuth about 4% lower, than the results reported herein. The OSS was positioned at the 30° position (rather than 45°) since the telescope is used more frequently near zenith than horizon.

Modal analysis was used in this phase of the design for a number of specific purposes:

1.) "Fully constrained" models (with stiffness across the encoder references of both altitude and azimuth drives) were used for comparison with the system as defined a year ago, and to verify that optimizing of the OSS for gravity effects had not degraded the modal performance. Locked encoder (or infinite) stiffness was used for the drives because of recent control system analysis and the belief that it provides a more accurate prediction of system performance with the high performance drives than does locked rotor.

2.) Frequency response modal analysis models with zero drive stiffness across the encoder reference of either drive were used for subsequent frequency response analysis to support control system analysis and design.

3.) Models of the OSS alone and combined with the fork under various support constraints were used to predict "twisting modes" within the OSS. This was done to help determine the best encoding configuration and method of control to be used on the altitude axis (ref 3.35 below).

3.3.1 Fully constrained modal analysis

The calculated modal performance using locked encoder drive stiffness simultaneously for both axes is summarized in Table 1. Modeshapes are shown in the graphics plots of Figures 17 through 20. A video presentation demonstrating the modeshapes is also planned.

Some improvement in modal performance has been made due to the stiffening of the upper azimuth support system (ref E305008), and the optimizing of the OSS for gravity effects (section 3.5 below). However, frequencies of modes significantly affected by drive stiffness should not be compared to those in the June 1990 report. The increase in these frequencies is much more a reflection of the use of a more accurate analysis criterion (locked encoder versus locked rotor) than it is of performance improvement.

It should be noted that a problem was encountered during the early processing of these finite element models. A software irregularity caused the full telescope modal analyses to exceed a temporary file size (approximately 67 megabytes) causing program termination. Although this problem is now being resolved by the finite element software vendor, the models as run had to be made slightly smaller. This was done by unmeshing the main truss beam elements, swapping simplified beam elements for the plate element secondary x-brace, and eliminating the first row of plate elements in the lower bearing pedestal (ref Figure 1). Of these changes, only the latter might have a nonconservative effect on the results. This was tested on an earlier version of the model which would run with the full pedestal, and the effect was found to be negligible.

While these three features (truss mesh, x-brace, and pedestal) are visually apparent on the graphics plots, the resulting frequencies are unaffected.

Detailed modeshape discussion is provided with Figures 17 through 20.

3.3.2 Frequency response analysis - simplified model

A Frequency Response Analysis (FRA) was performed for each control axis of the telescope. The FRA requires that a modal analysis be made with the control axis unconstrained but with elements representing the drive inertia and stiffness properties in place for subsequent excitation by an applied sinusoidal force. The FRA program then determines the magnitude response (radians/N-m) and phase response (degrees) at each specified input excitation frequency. The response is calculated for every node in the finite element model, so that if one looks at the encoder reference node(s), the response at the encoder is determined for an excitation at the drive motor.

Prior to performing the FRA on the WIYN highly meshed finite element model, the process was tested on a much simpler model. Since the Magellan Project had recently performed a similar frequency response analysis[2] based on a simplified math model of the system, this was chosen to test the FEA/FRA method. This work is summarized in the appendix ("Magellan Project 8 Meter Telescope - Frequency Response Analysis by Finite Element Analysis").

As shown in the magnitude response plot, and keeping in mind that the first resonance peak is an artifact, the correlation between the FEA and math methods was found to be excellent. In this highly simplified model the true first resonance was determined to be the first azimuth free-boundary mode, or that in which the system twists around the azimuth axis with the OSS and azimuth systems out of phase. The second true resonance was found to be that of the drive shaft of the direct friction drive vibrating against the drive disk. The first locked encoder resonance was absent. The subsequent phase response plot then indicates excellent control properties in the case of the Magellan simplified system, since the large negative phase doesn't occur until 250 hz.

3.3.3 Azimuth frequency response analysis

After confirming the accuracy of the finite element program on this simplified model, the method was then applied to the WIYN detailed finite element model. As shown in Figure 15, the azimuth axis rotation was unrestrained in the modal analysis, and then excited for the frequency response analysis. The results of the altitude (FRA) modal analysis are shown in Table 3. The (FRA resonance) modeshape would be difficult to visualize from a graphics plot, but is best described as having two effects: 1.) the rotation of the OSS and upper fork area around an axis approximately coincident with the OSS local Y axis (which is perpendicular to the plane formed by the altitude and optical axes) and 2.) rotation of the lower end of the fork (including the azimuth disk) around the azimuth axis. While the first effect is dominant, close inspection of the animated modeshape shows the second is significant. This resonance occurs at 25.4 Hz.

Note that this is not the same modeshape as that found in the Magellan simplified model. It is believed that this is due to the fact that this is simply a lower frequency (azimuth-coupled) mode than the first free boundary mode. The modal analysis, calling for the lowest 16 frequencies, gave modes through 34.3 Hz. The first free boundary mode is certainly above this, and therefore the program cannot recognize it as a resonance in the frequency response analysis.

While a discussion of the control system analysis and design is beyond the scope of this report, the magnitude and phase response plots from the servo design report[3] are presented in the appendix.

3.3.4 Altitude frequency response analysis

As shown in Figure 16, the altitude axis rotation was unrestrained with beam elements and masses installed to simulate the drive properties and allow for subsequent excitation in the FRA. The results of the altitude (FRA) modal analysis are shown in Table 2. The first resonance was fore-aft translation (9.4 Hz), shown in the graphics plot, Figure 21. The second resonance, vertical translation (25.4 Hz) is shown in Figure 22.

The magnitude and phase responses are shown in the appendix, and the servo design summarized in a separate report[4]. Again, the "locked encoder" resonance is not present.

3.3.5 "Twisting modes"

Modal analysis of the OSS alone and mounted on the fork were performed to better understand how the two altitude drives should be controlled. The concern was that the compliance of the OSS across the axis might cause local resonance to adversely couple with the control for the two altitude drives. This was then imagined as a "twisting mode" along the altitude axis of the OSS. Analysis showed that the frequency of this mode must be very high (above 43 Hz reached by modal analysis). However some modes do involve unsymmetric motion at the two altitude drive locations. It was concluded that the lowest of these was 33 Hz and that this is sufficiently high as to not be a problem.

3.4 STATIC ANALYSIS - WIND LOADING

Effects of wind loading on the complete telescope structure are shown in Figures 23 through 25 and in Table 4. Front and side wind loading was applied in the zenith and horizon-pointing attitudes.

Without the benefit of a wind tunnel test (or other more detailed analysis beyond the scope of this effort) wind pressure loading was simply applied to all members exposed to the wind. This was done as if the telescope, above the observing floor, were exposed to a free air flow velocity of 15 mph, with a 7,000 ft elevation air density. The actual pressure loading used was 0.46 psf (pounds/ft^2). From recent testing at APO this should generally be representative of about a 45 mph ambient wind remote from the enclosure.

Absolute displacements of nodes representing the optics are included in the Appendix. The primary pointing errors and optical misalignments are shown in Table 4. Although evaluation of these results is beyond the scope of this report, it can be said that the optical misalignments under these assumptions have a negligible effect on image quality. The pointing errors, while significant, are much lower than predicted earlier[5] due mostly to the more realistic use of locked encoder drive stiffness, and partly to the stiffened upper azimuth support system. All of the steady-state component, and some of the dynamic component of the pointing error due to wind will be removed by the control system under closed-loop servo control.

3.5 STATIC ANALYSIS - ROTATING THROUGH THE GRAVITY FIELD

Model OSS57 (and earlier optimizations) were created to determine optical misalignments due to rotating through the gravity field. This was done by applying negative zenith and positive horizon gravity components. An exaggerated deflected plot is shown in the center of Figure 26. The absolute motions of nodes representing the optics are included in the appendix. The resulting relative motions are provided in Table 5.

It was decided that the primary mirror would be held fixed in its cell using the mirror support system controls. In this way, the primary pointing should be more reliably defined than allowing it to move under the significant compliance of the support system itself.

The alignment of the optics was accomplished in two steps:

1.) First-order optimizing of the secondary end (increased main truss section, decreased square frame section and other members in the secondary center structure, and increased vane sections) caused the secondary end to sag less and rotate favorably.

2.) Changing the primary end truss geometry and reducing its section properties caused it to rotate favorably and sag more, pointing the primary mirror directly at the secondary with both at horizon.

The net effect of the above is that the secondary and primary remain collimated as the OSS rotates from zenith to horizon. Some residual defocus currently exists (due to the same motion) which can be minimized in the detail design phase.

4.0 SUMMARY AND CONCLUSIONS

The preliminary design has continued in this phase. Structural performance has been improved in some cases and better understood in others. Mechanical systems (instrument rotator, direct friction drives, counterweights, etc.) are better defined and therefore closer to becoming good detail designs.

Some recent changes in the structural design will necessitate updating of some of the finite element analyses in the detail design phase. However, sufficient analysis has been performed to say with confidence that there will be no surprises, and that the system should be capable of excellent pointing and tracking performance.

5.0 REFERENCES

1. Gunnels, Steven M., "Direct Friction Drives", Magellan Project Report No. 18, March, 1990.

2. Schier, J. Alan, "Boundary Conditions, Vibrational Modes, and Frequency Responses: What's Important for Telescope Performance?", Magellan Project Report No. 29, February 1991.

3. Schier, Alan, "WIYN Azimuth Axis Servo Design", WIYN 3.5 Meter Telescope Report No. WODC 02-08, May, 1991.

4. Schier, Alan, "WIYN Altitude Axis Servo Design", WIYN 3.5 Meter Telescope Report No. WODC 02-09, May 1991.

5. "Engineering Report - Preliminary Design Study - WIYN 3.5 Meter Telescope" by L & F Industries, June 1990.

FINITE ELEMENT ANALYSIS - SUMMARY OF RESULTS

TABLE 1

NATURAL FREQUENCIES AND MODESHAPES - FULLY CONSTRAINED

The following modal performance is from model WIYNTM60, the complete telescope with OSS 30° from zenith, conventionally constrained ("locked encoder", or infinite drive stiffness). The four primary modeshapes are shown in Figures 17 through 20. Additional discussion can be found in the body of the report.

MODE	FREQUENCY Hertz	MODESHAPE DESCRIPTION
1	8.2	Lateral Translation
2	8.8	Fore-Aft Translation
3	14.7	Altitude Disks Out-of-plane Bending
4	14.8	Altitude Disks Out-of-plane Bending
5	16.4	Secondary Assembly Rotation about the Optical Axis (manual calculation not recently updated)
6	17.3	Locked Encoder Altitude
7	21.0	Main Truss Tube Bending (estimate of local mode)
8	22.4	Locked Encoder Azimuth
9	22.9	Altitude Disks
10	23.0	Altitude Disks
11	25.2	Vertical Translation
12	27.4	Secondary Lower X-brace
13	29.0	OSS Rotation 45° Axis
14	32.8	Secondary Piston/Nasmyth Instruments
15	33.1	(similar to mode 14)
16	33.7	(similar to mode 15)

TABLE 2

NATURAL FREQUENCIES AND MODESHAPES ALTITUDE FREQUENCY RESPONSE

The following modal performance is from model WIYNTM35, the complete telescope with OSS 30° from zenith, with zero altitude drive stiffness, locked encoder azimuth stiffness. Only primary modes are listed. The two modeshapes which represent resonant peaks in the frequency response analysis are shown in Figures 21 and 22. Additional discussion can be found in the body of the report.

MODE	FREQUENCY Hertz	MODESHAPE DESCRIPTION
1	0.0	(Rigid Body Altitude)
2	8.1	Lateral Translation
3	9.4	Fore-Aft Translation (FRA Resonance)
4	20.6	Locked Encoder Azimuth
5	25.4	Vertical Translation (FRA Resonance)

TABLE 3

NATURAL FREQUENCIES AND MODESHAPES AZIMUTH FREQUENCY RESPONSE

The following modal performance is from model WIYNTM36, the complete telescope with OSS 30° from zenith, with zero azimuth drive stiffness ("free boundary azimuth"), and locked encoder altitude stiffness. Only primary modes are listed. The modeshape which represents a resonant peak in the frequency response analysis is mode 5, OSS rotation about its local Y-axis. Additional discussion can be found in the body of the report.

MODE	FREQUENCY Hertz	MODESHAPE DESCRIPTION
1	0.0	(Rigid Body Azimuth)
2	7.8	Lateral Translation
3	8.3	Fore-Aft Translation
4	16.8	Locked Encoder Altitude
5	25.4	OSS Local Y-axis Rotation (FRA Resonance)
6	26.6	Vertical Translation

TABLE 4
WIND LOAD DEFLECTIONS

The following data are from models WIYNTZ58 and WIYNTH59 (and data reductions made from these results) and are based upon a 15 mph wind *acting upon the telescope structure.* It is expected that this is generally representative of a 45 mph ambient wind remote from the enclosure. Graphics plots of the deflected structure are provided in Figures 23 through 25. Absolute deflection data is included in the Appendix. Additional discussion can be found in the body of the report.

Attitude/Wind Direction	Primary Pointing Error	Secondary Decenter	Misalignment Rotation
zenith/front wind	.43 arcsec	2.64 microns	.05 arcsec
zenith/side wind	.19 arcsec	2.3 microns	.023 arcsec
horizon/front wind	.32 arcsec	.33 microns .72 microns piston	.04 arcsec X .05 arcsec Z
horizon/side wind	.06 arcsec	2.2 microns	.02 arcsec

TABLE 5
GRAVITY MISALIGNMENTS

The following results are from model OSS57. It has been assumed that the mirror support system will maintain a fixed position of the mirror relative to the cell referenced at the three "hard points". If optics are aligned at zenith, these misalignments will develop between the secondary and primary mirrors as the OSS is rotated to horizon. Motions are referenced to the secondary mirror vertex. Absolute deflection data is included in the Appendix.

NET DESPACE (PISTON)	NET Y-DECENTER (SAG)	NET X-DECENTER	NET TILT (ROTATION)
68 microns separate	0.54 microns at targets 2ndry below primary	3.54 microns at targets secondary +X	0.004 arcsec X 2ndry points back below primary
	0.12 microns SMT/primary axis	3.52 microns SMT/primary axis	3.26 arcsec Y 2ndry points to positive X

Primary axis and tertiary mirror target sag approximately 240 microns below altitude axis.

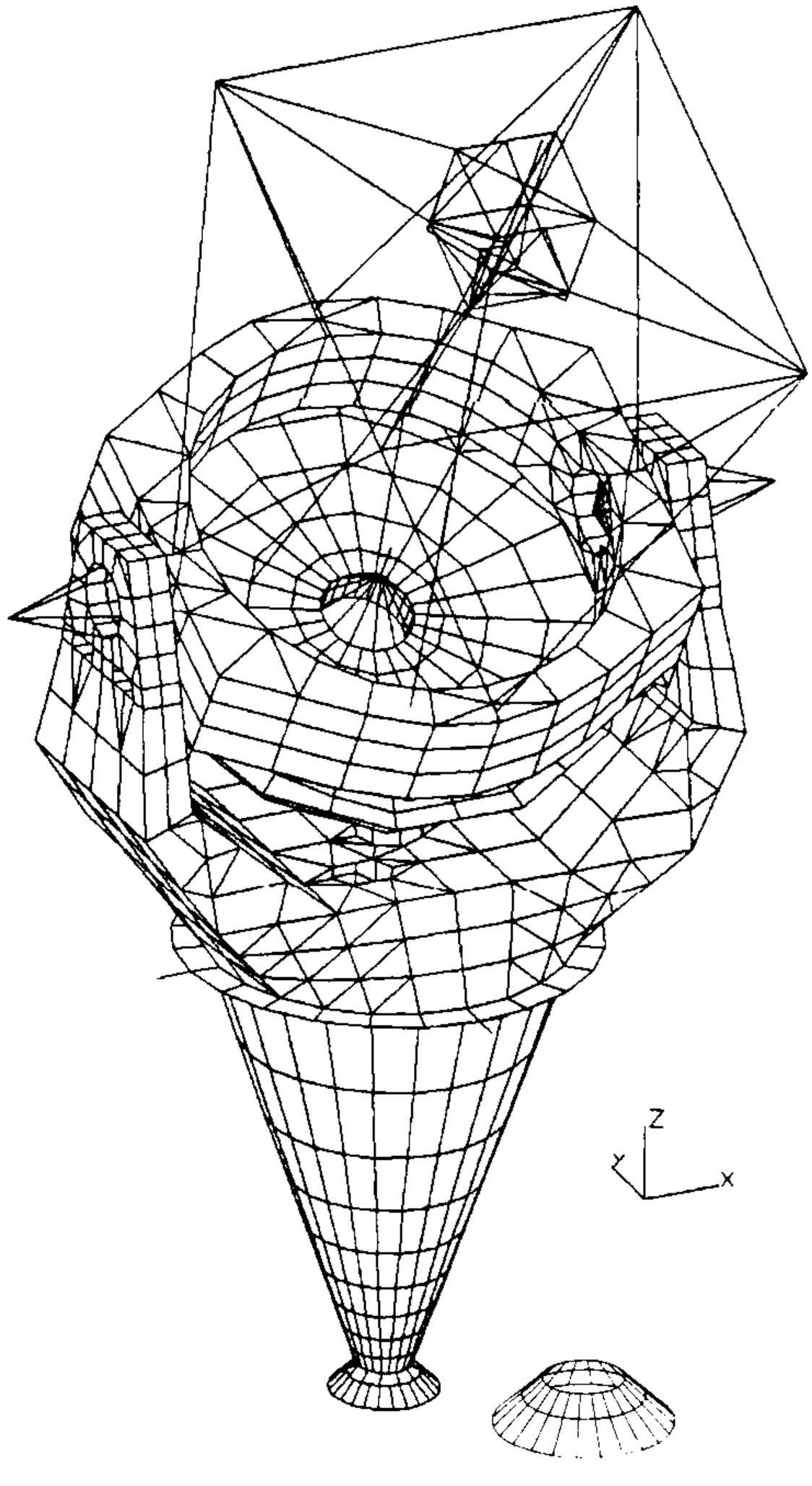

FIGURE 1 - Model WIYNTM60, the complete telescope model used for modal analysis, shown with hidden lines removed. OSS is 30° from the zenith attitude. Some elements, such as the lower bearing pedestal and secondary center structure lower X-brace were simplified or removed in order to reduce the size of the finite element model (see discussion in body of report). Full pedestal is shown adjacent to lower end of model.

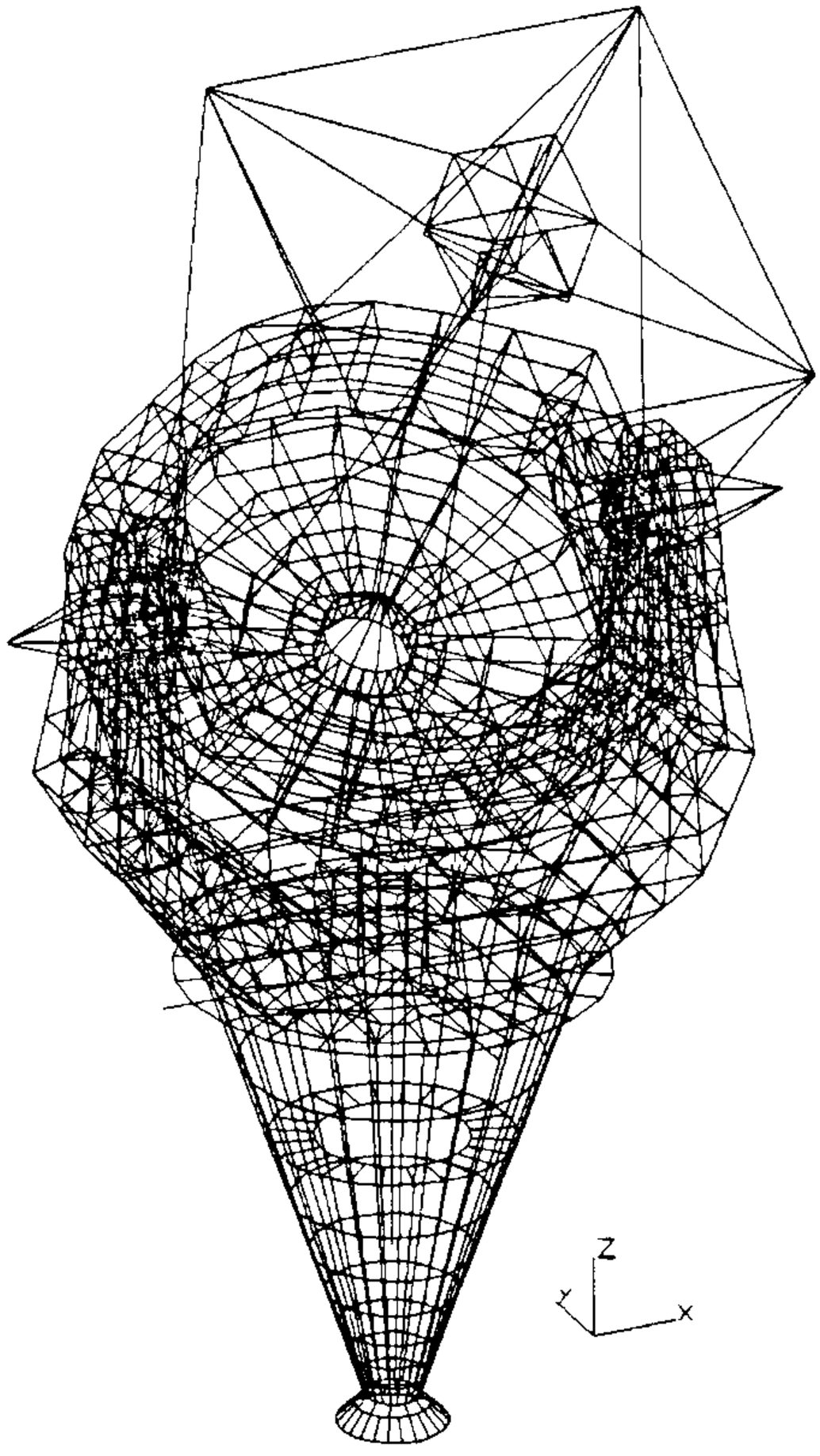

FIGURE 2 - Model WIYNTM60 without hidden lines removed.

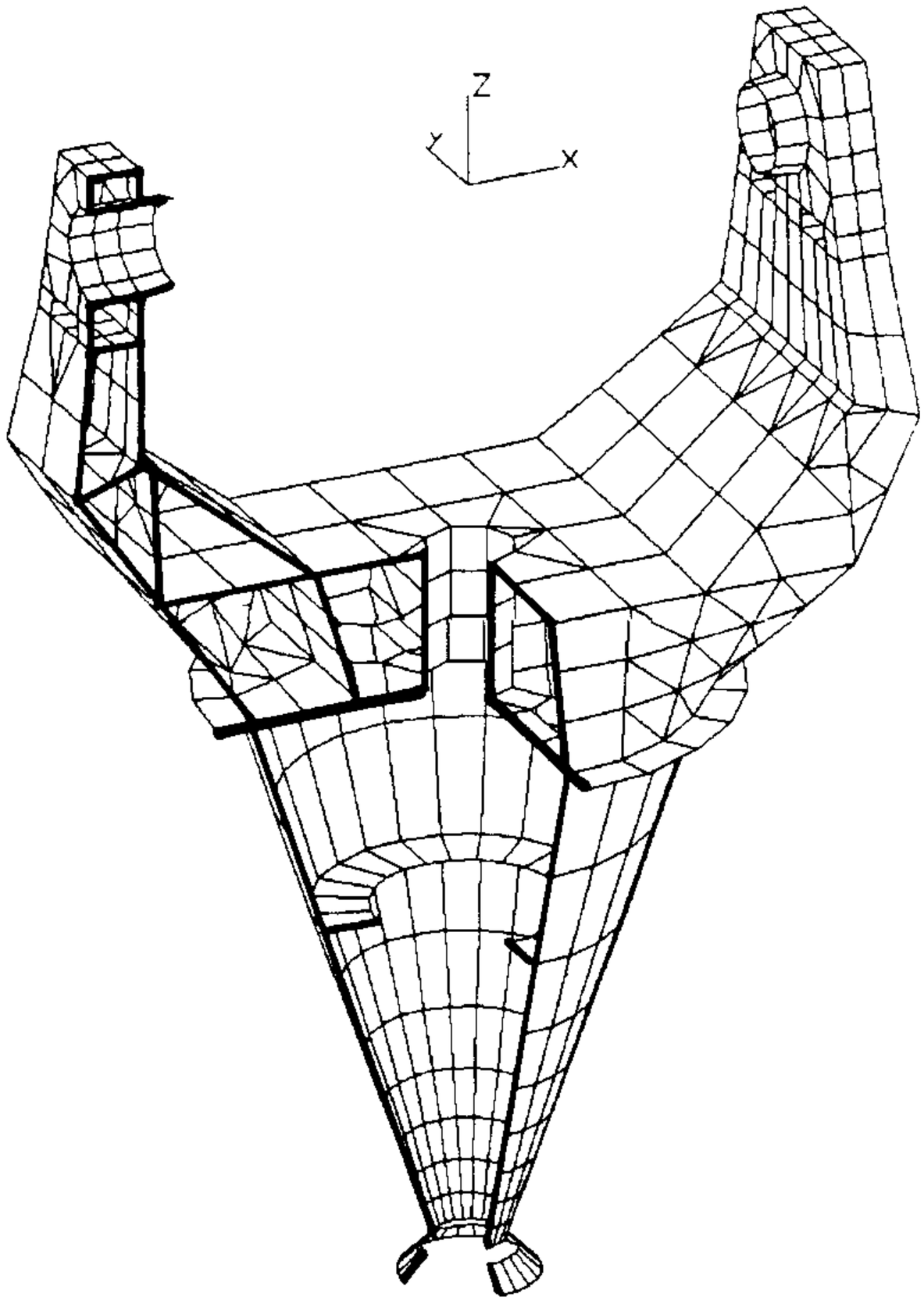

FIGURE 3 - Cutaway view of the fork. Mechanical (bolted) joints are located as described in subsequent graphics plots.

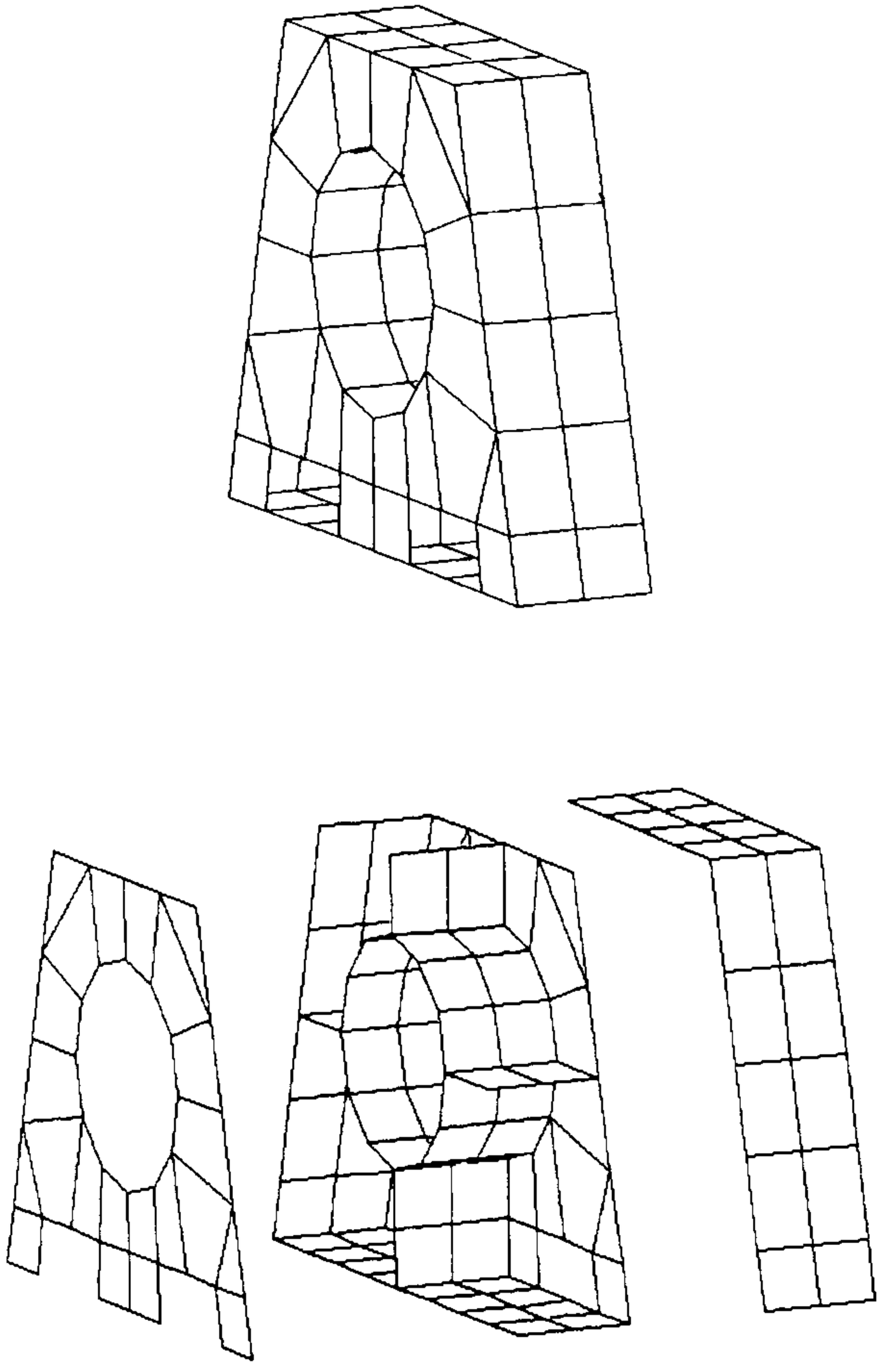

FIGURE 4 - Exterior and exploded views of one pillow block, which bolts to the top of each fork tine. Bolting access holes are provided near the bottom of the large vertical plates. All plate elements in the model were 1/2" thick except the axle support tube (2.25") and the bottom plate, made 2.75" thick to represent the combined thickness of the pillow block bottom plate and tine top plate.

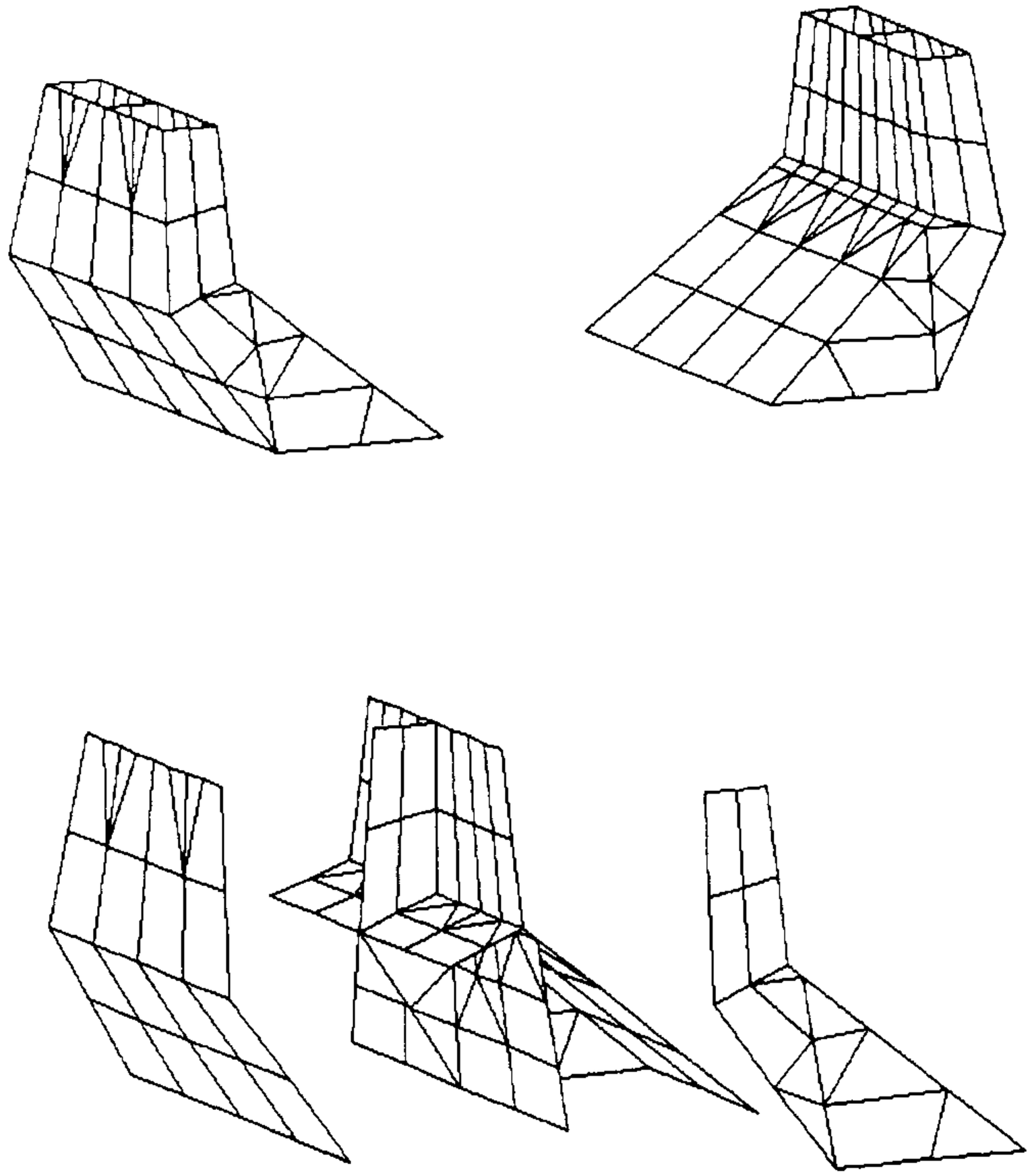

FIGURE 5 - Exterior and exploded views of the fork tines. These are planned as being integral with the horizontal "throat" of the fork (also referred to as the "base") in a single weldment. All plates were modelled as 1/2" thick except the internal slanted plate tieing the inner and outer plates at the "knee" of the bend, which was modelled as 3/4" thick.

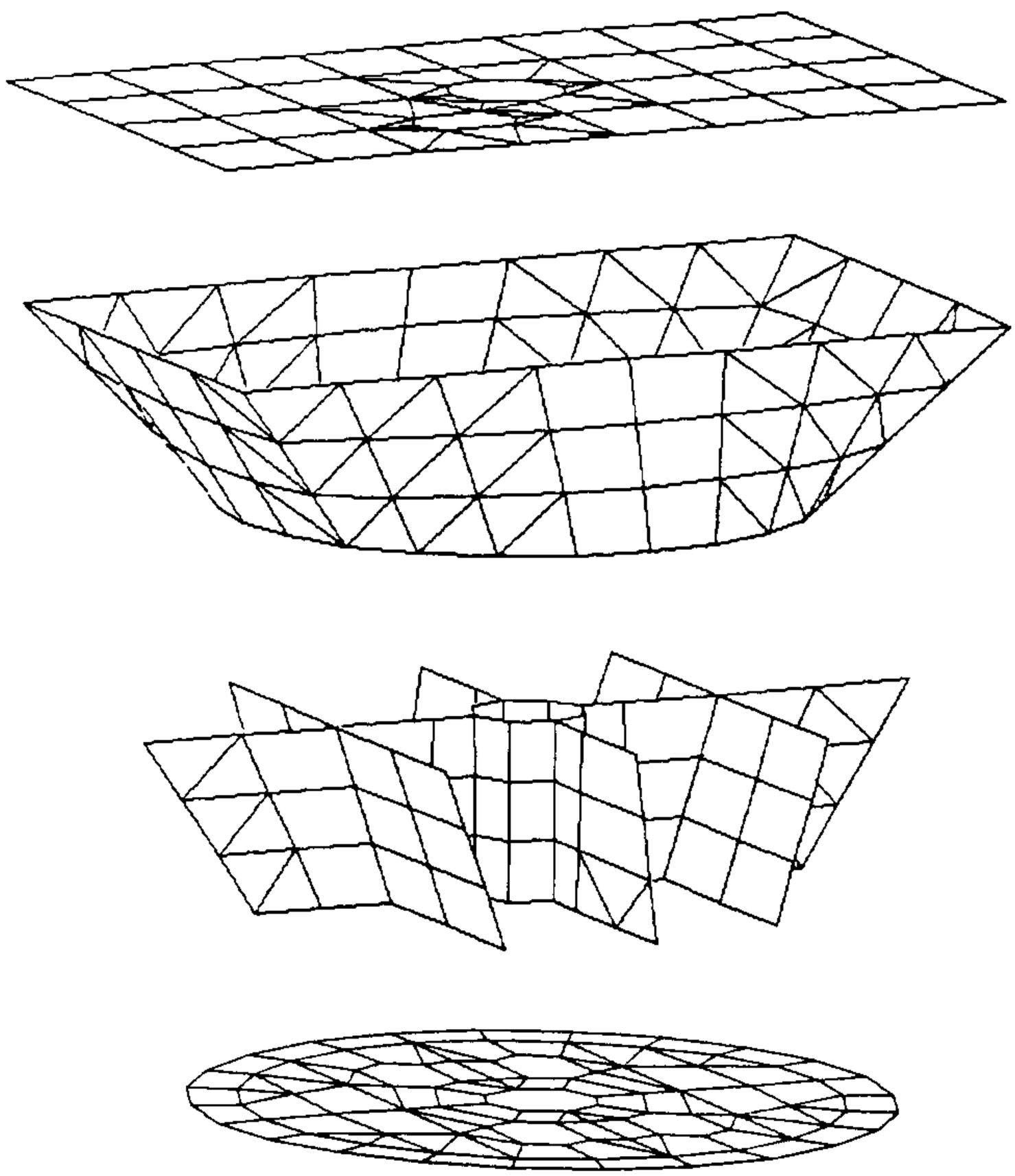

FIGURE 6 - Exploded view of the "base" portion of the fork. The top horizontal plate is 3/4" thick and includes a 15" x 22" hole for personnel access into the fork and lower cone. The outer shell is a transition which is rectangular at its top end and circular at its lower end, and is 3/4" thick. All internal plates are 1/2" thick except the central tube for utilities clearance, which is 1/4" thick. The bottom plate of the real weldment is planned as 1 3/4" thick except near the edge, where it is machined to 1 1/8" thick. The azimuth drive disk in the real telescope is planned as 1 5/8" thick in the central area and 2 1/2" thick at the rim. These two plates were combined in the model as a single 2" thick plate with a steel modulus, but artificially high mass density. Note that the center of the bottom plate ties to the internal webs and the central tube, and that there are four 15" x 22" oval holes to allow personnel access to the base (from the cone) for routing utilities, etc.

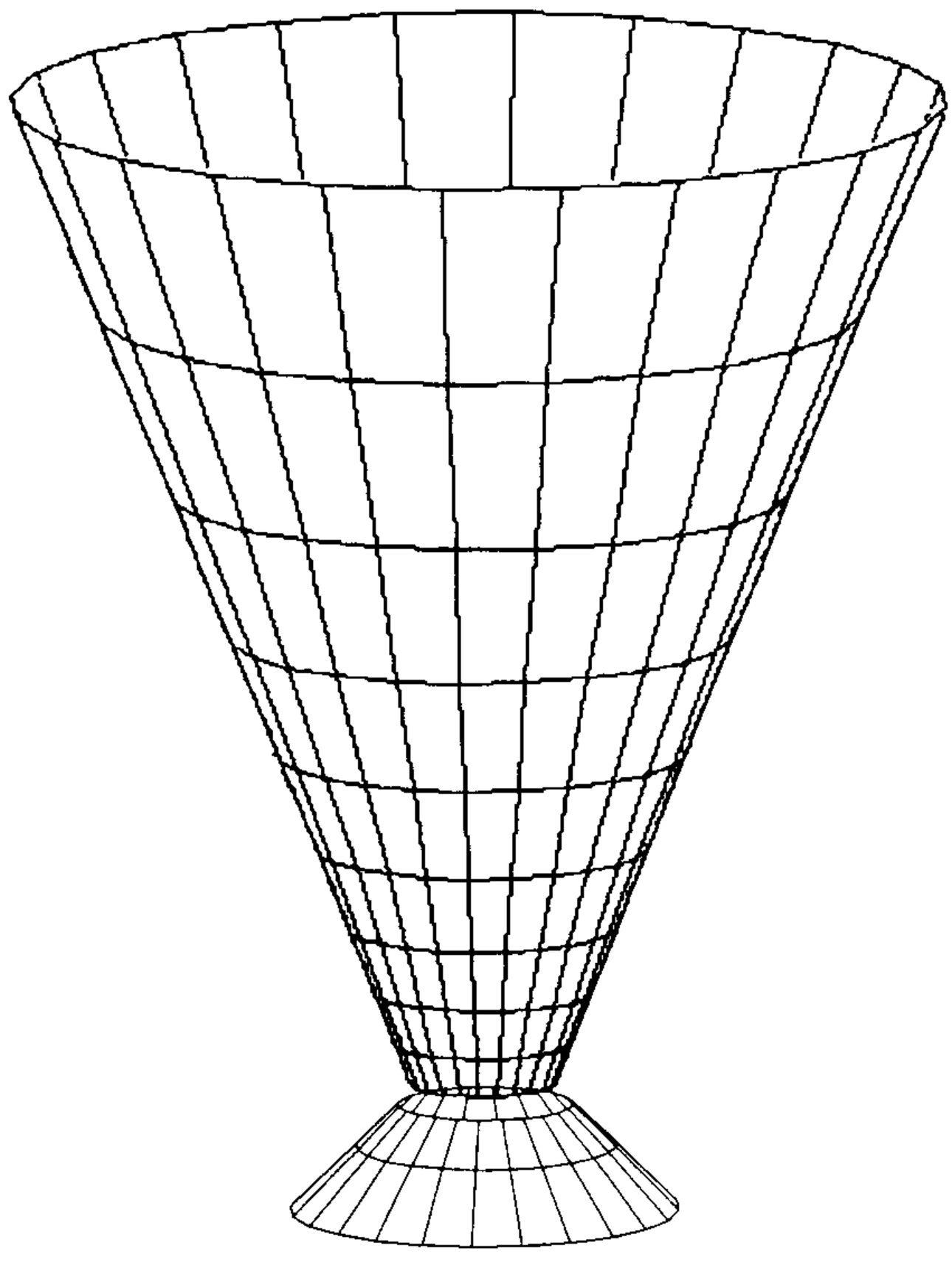

FIGURE 7 - Cone and lower bearing support pedestal. All elements are 3/4" thick except that the pedestal and lower area of the cone are 1" thick. An internal circular ring was added in the cone to minimize its distortion for certain modeshapes, and which would be required in the real telescope as a manufacturing aid.

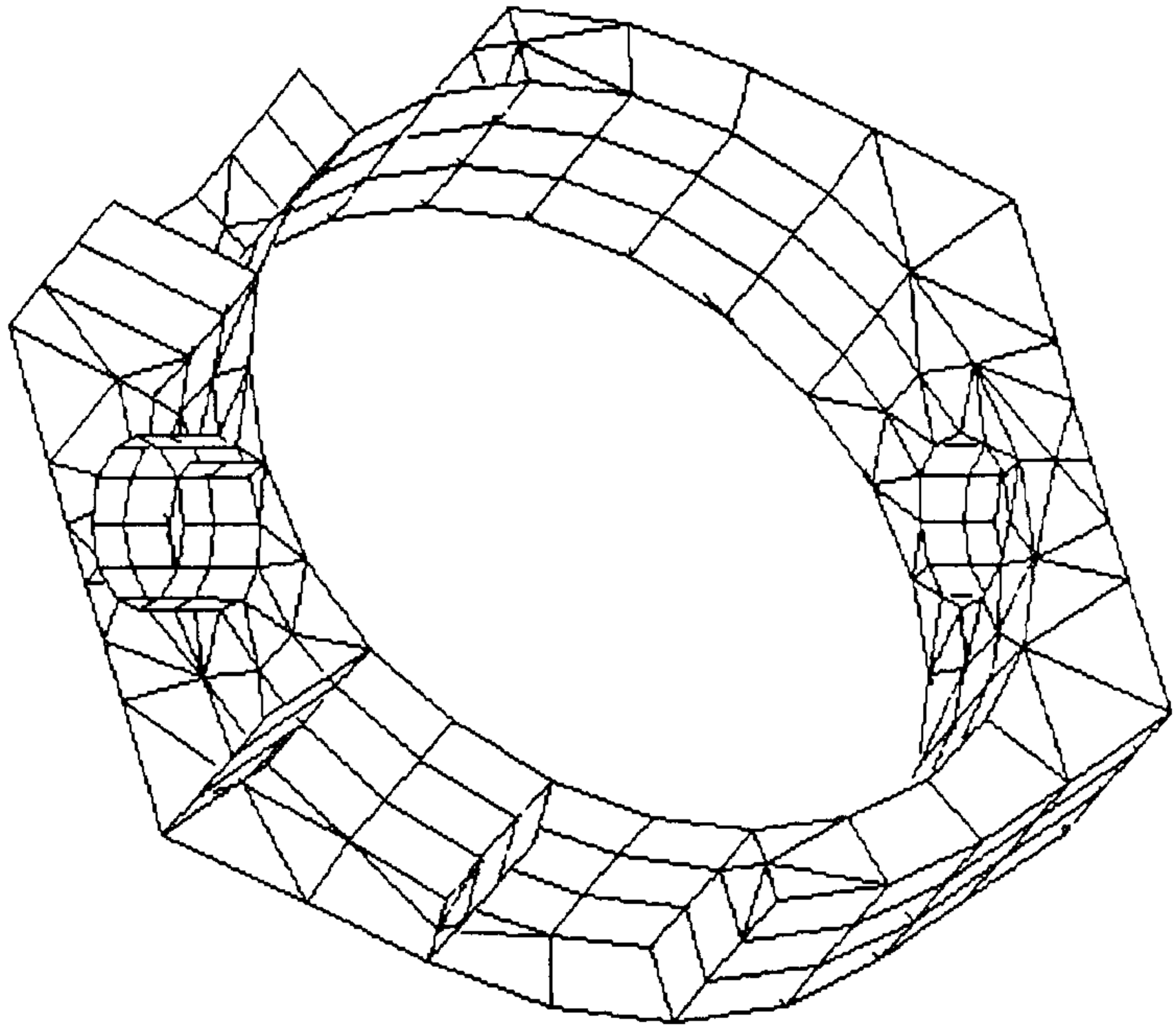

FIGURE 8 - Center section of the Optics Support Structure, with external plates removed in the near half. All plates are 3/8" thick except that all internal gussets are 1/2" and the bearing support tube has varying thickness as shown on drawing E305007 sheet 2. Note that the third instrument position to be mounted on the top side of the center section was not modelled, on the assumption that its effect is negligible. Such an effect would likely be included in the final (detail design) finite element model.

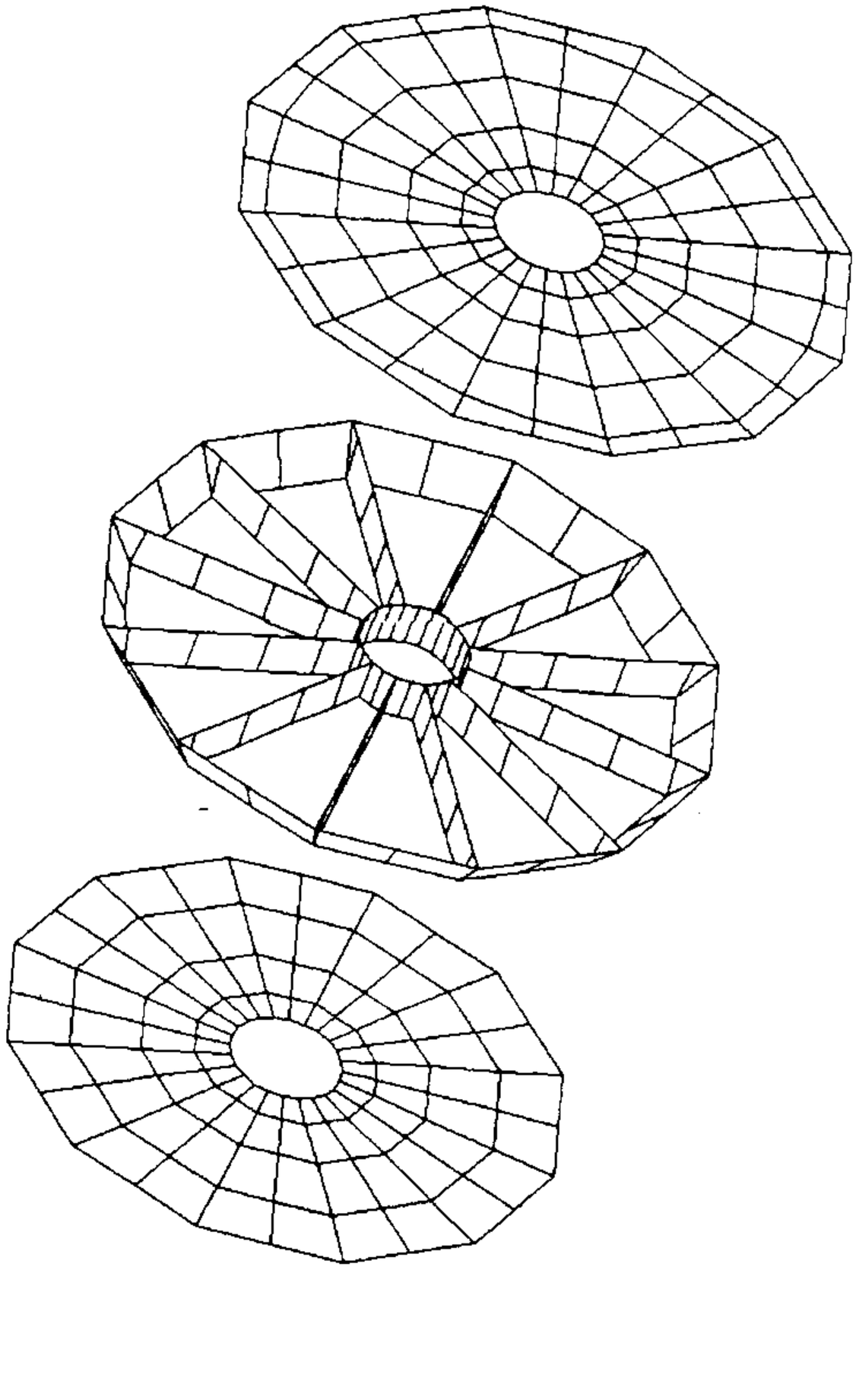

FIGURE 9 - Simplified mirror cell used in all models in this phase of the finite element analysis, which assumed that mirror support system maintains mirror position as fixed relative to cell.

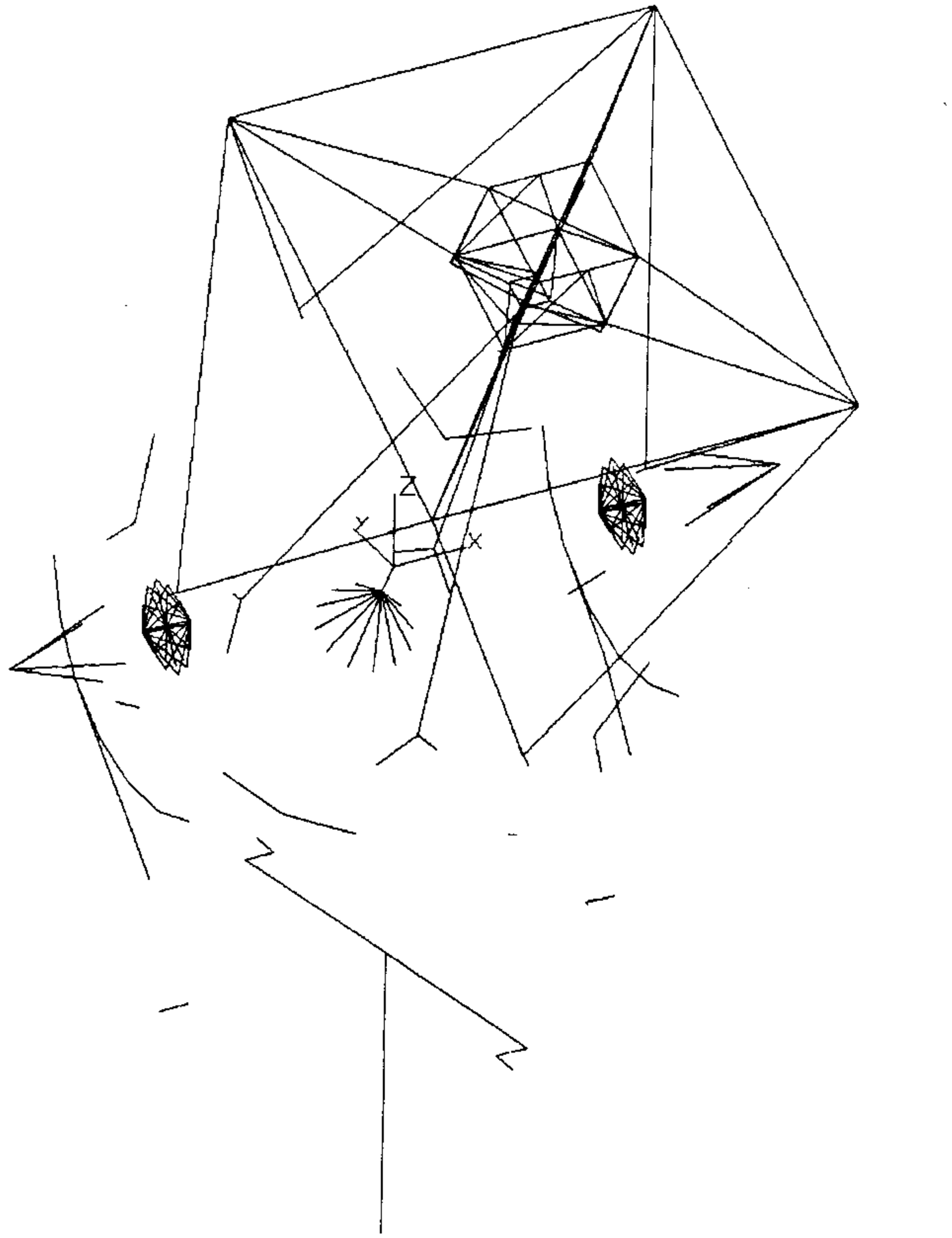

FIGURE 10 - The 295 beam elements in model WIYNTM60, the optimized modal analysis model. Many elements are used to define spring rates, such as the altitude and azimuth bearings. Detailed descriptions are included in the following graphics plots.

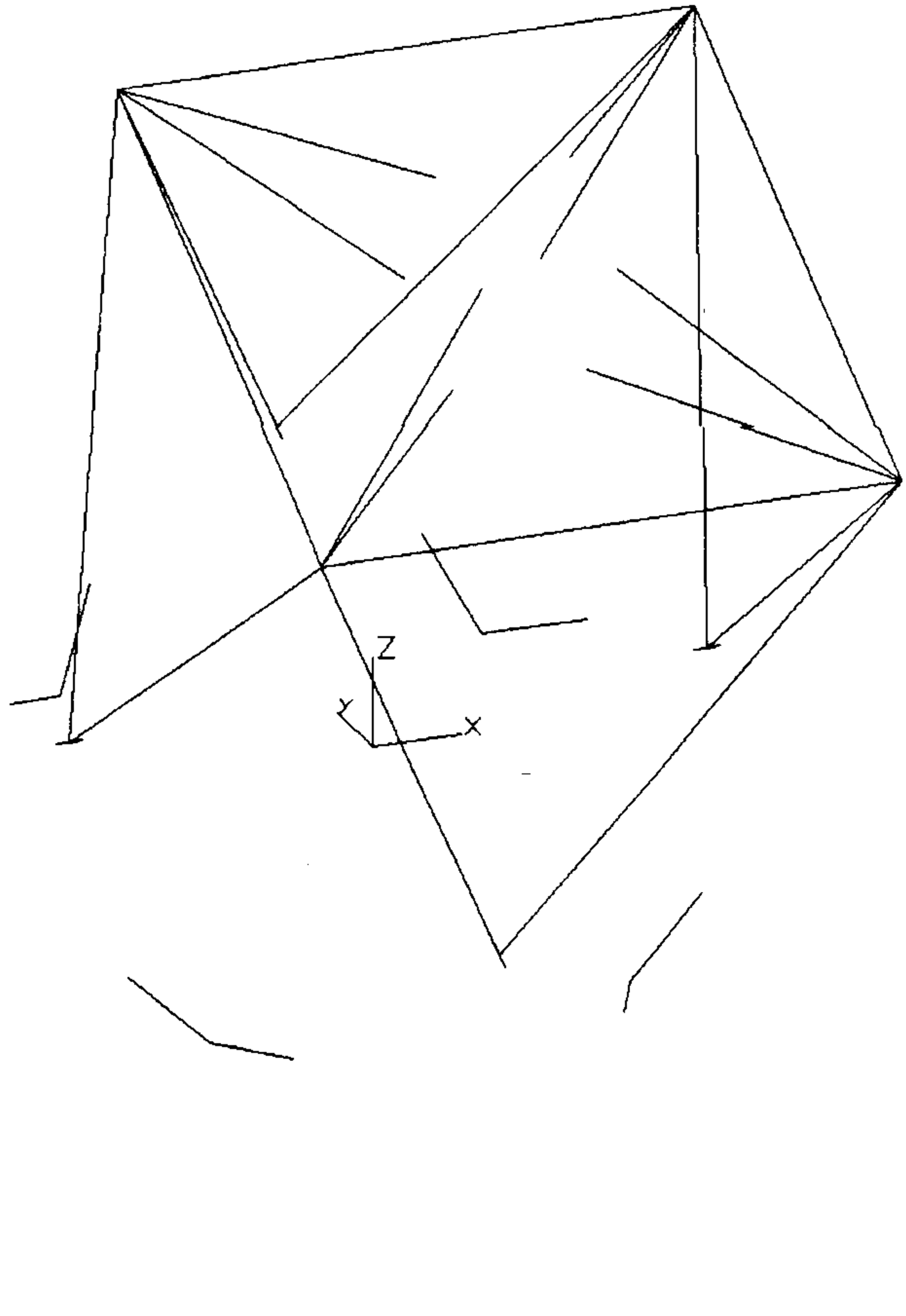

FIGURE 11 - The beam elements used to define the primary and secondary end main trusses and secondary vanes. The primary truss members are used to point the primary end at the secondary vertex as the OSS rotates through the gravity field. Primary truss members are 2 3/4" outside diameter x 1/4" wall tubing. Secondary main truss is 4 1/2" o.d. x 1/2" wall, square frame is 4" o.d. x 3/8" wall, vanes are 1/2" x 3 1/2" and 1/2" x 2" flat bar.

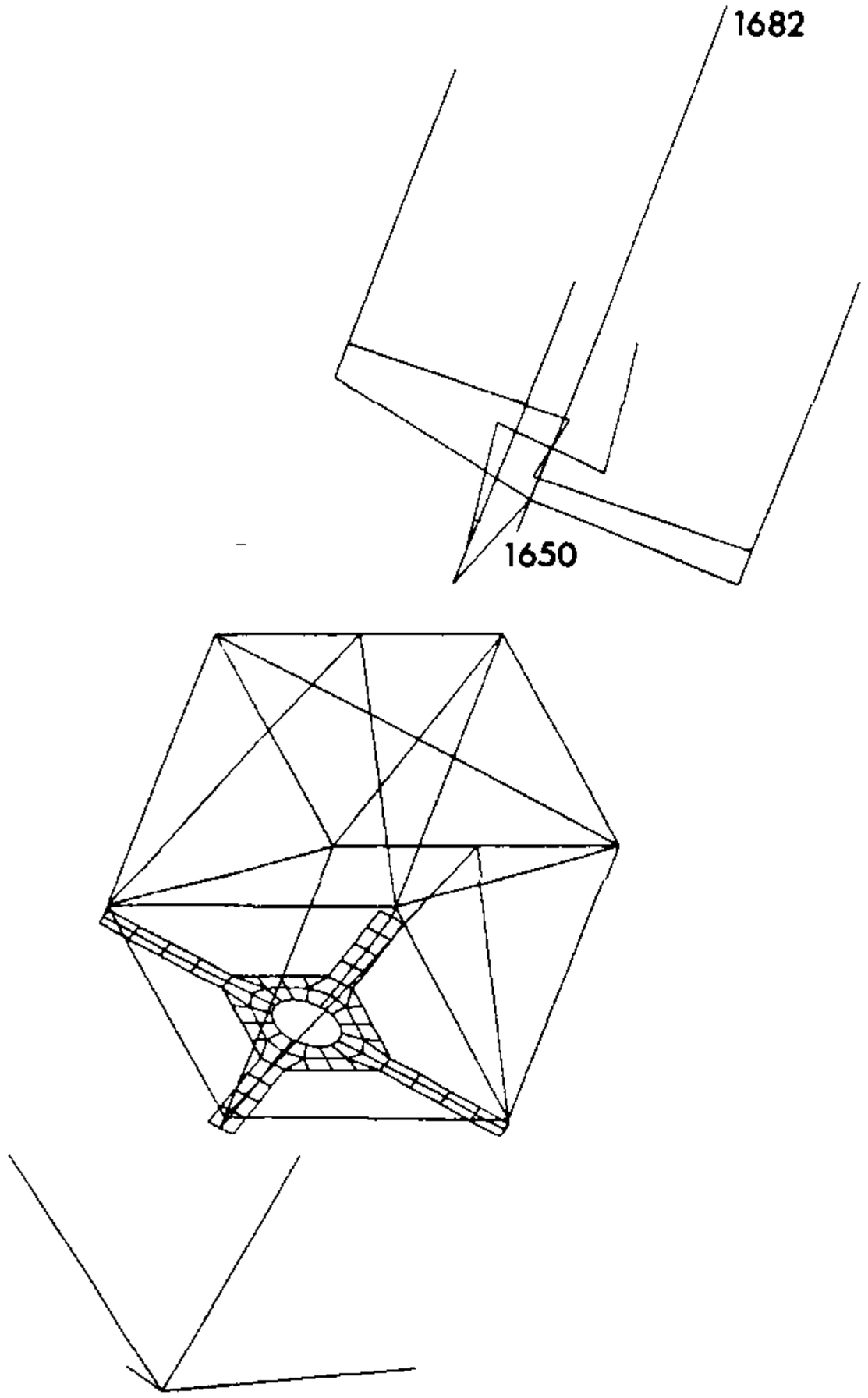

FIGURE 12 - The secondary center structure with the secondary mirror and supports removed and shown above, and the baffle shown below. Baffle is non-structural (used only to distribute nodal load representing weight of, or wind on baffle). Center structure beam elements were: 3 1/2" o.d. x 3/16" wall axial corner members, 2 1/2" x 1/4" wall square tube end frames, and 2" x 1/4" wall square tube edge plane braces. Top end x-brace was 1/2" x 2" flat bar, while 3/8" thick plate elements were used for lower end x-brace. The secondary mirror and cell were modelled as rigid. Note the unsymmetrical 3-point axial support of the secondary (3 axial flexures), which has been verified as having acceptable gravity and wind performance. Node 1650 is the secondary mirror target (secondary vertex), while node 1682 is a projection of the axis of the secondary mirror back to the "zero coma" point. (These node numbers for model WIYNTZ58, the zenith wind loading model).

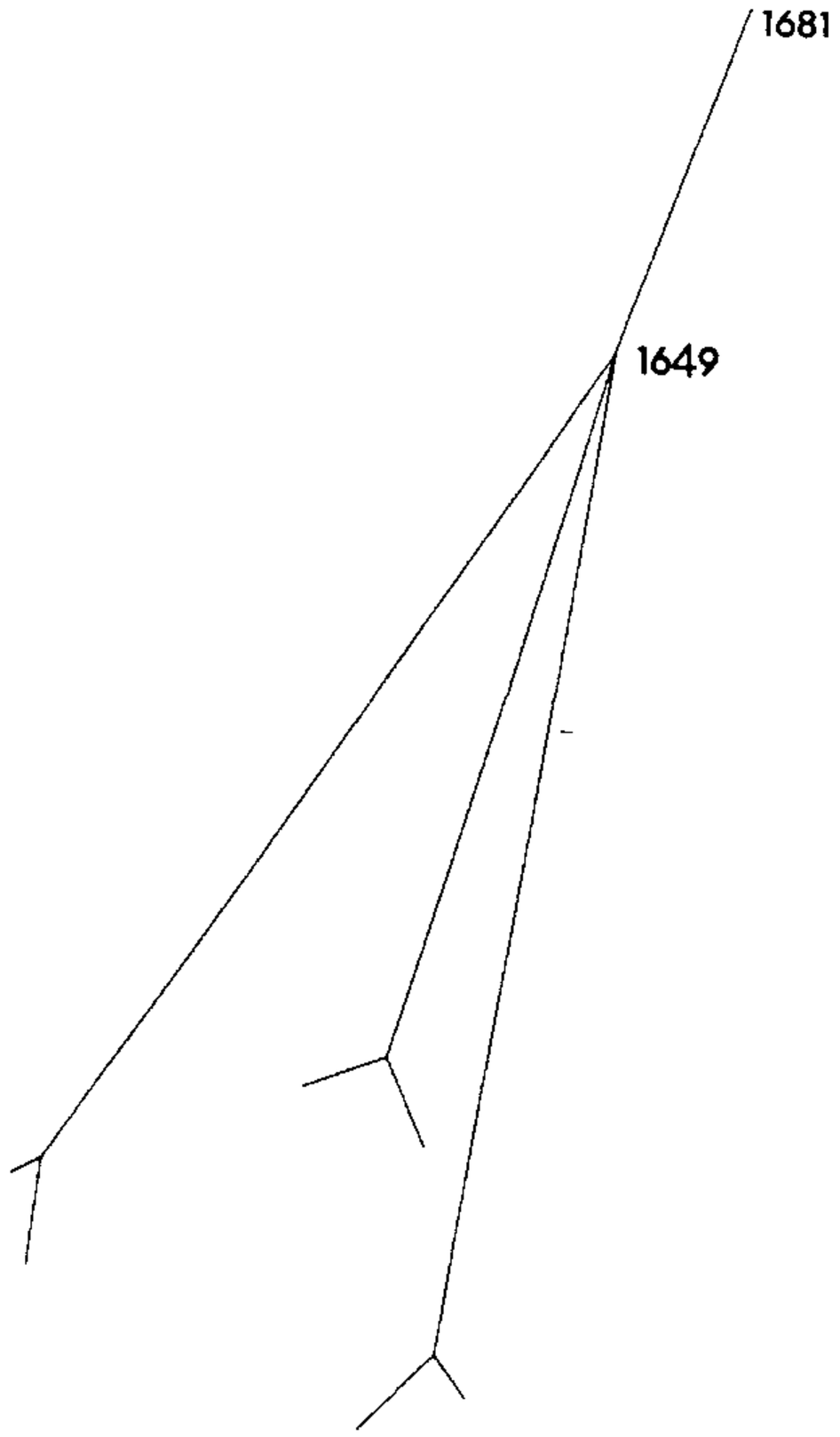

FIGURE 13 - The primary mirror target, node 1649 and primary axis at the zero coma point, node 1681, taken from WIYNTZ58 to determine optical misalignments due to zenith wind loading. The tripod attaches to cell at the three "hard points" of the mirror support system.

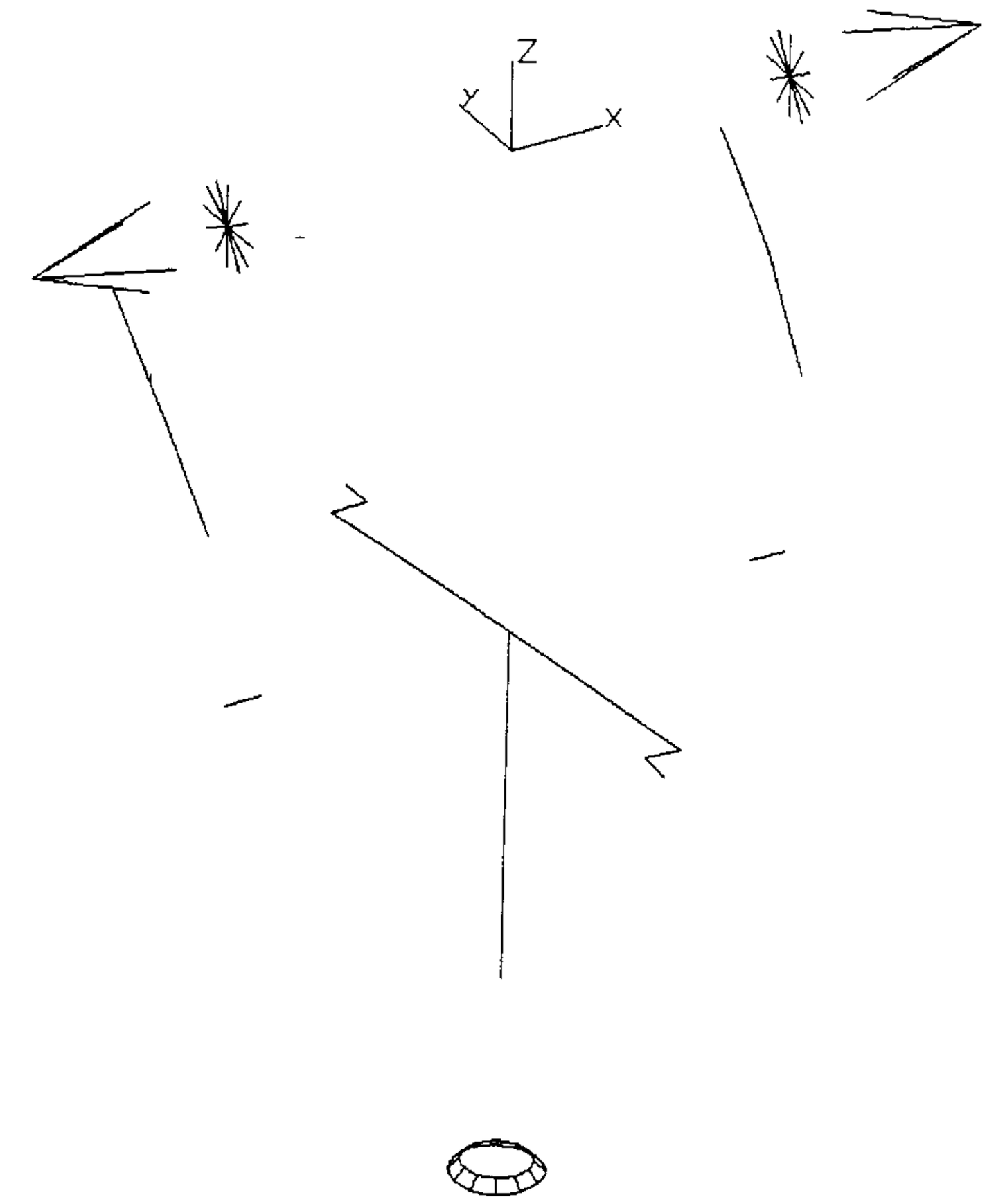

FIGURE 14 - All beam elements associated with the fork structure in models WIYNTZ58, WIYNTH59, AND WIYNTM60. Elements are (starting at the top of the view and working inward and downward): Nasmyth instruments, altitude bearing adapters, altitude drives, altitude drive support beams, upper azimuth radial supports, azimuth drive torsional system, and azimuth lower bearing and support rings. Altitude and azimuth "locked encoder" stiffness was used in these analyses (virtually infinite stiffness across the encoder references). Upper azimuth radial stiffness used was 1.34E6 lbs./in. for each drive and idler unit (up from 1.13E6 in the 1990 preliminary design). The lower bearing stiffness used was 5.57E7 lbs./in. (thrust stiffness component), based upon an SKF No. 29292 spherical roller thrust bearing.

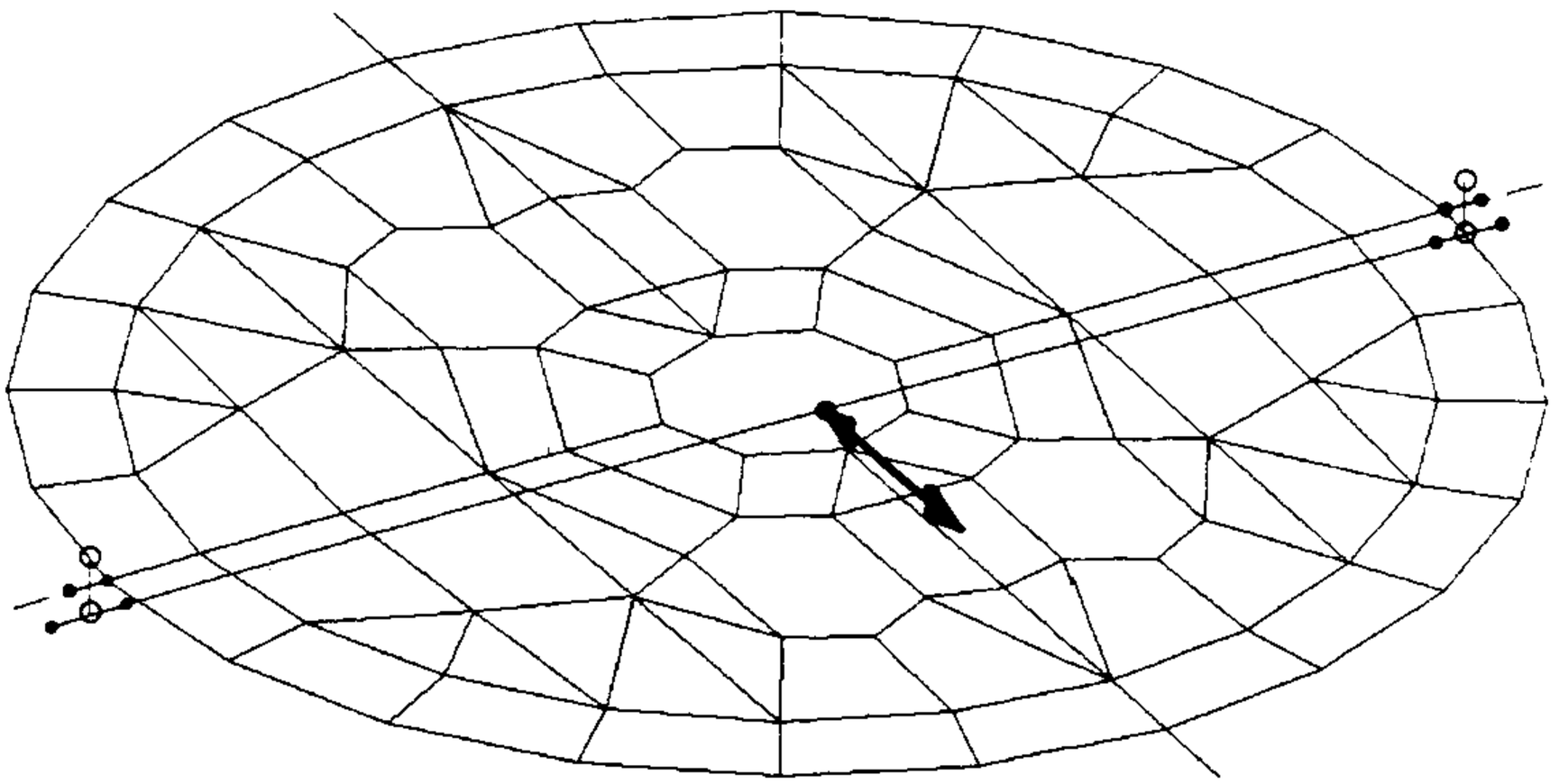

FIGURE 15 - A quartering view of the azimuth disk and azimuth drive excitation system used in model WIYNTM36, the modal analysis model used for subsequent frequency response analysis. A rigid weightless beam (whiffle tree) was used to distribute the excitation force equally to the rotor of the two drive motors. Whiffle tree connects to right side of left rotor and right side of right rotor as shown here. Drive shafts (drive roller, shaft, and motor rotor) were modelled with same inertial and stiffness properties as that expected for the real friction drive units. See body of report for additional discussion of the frequency response analyses.

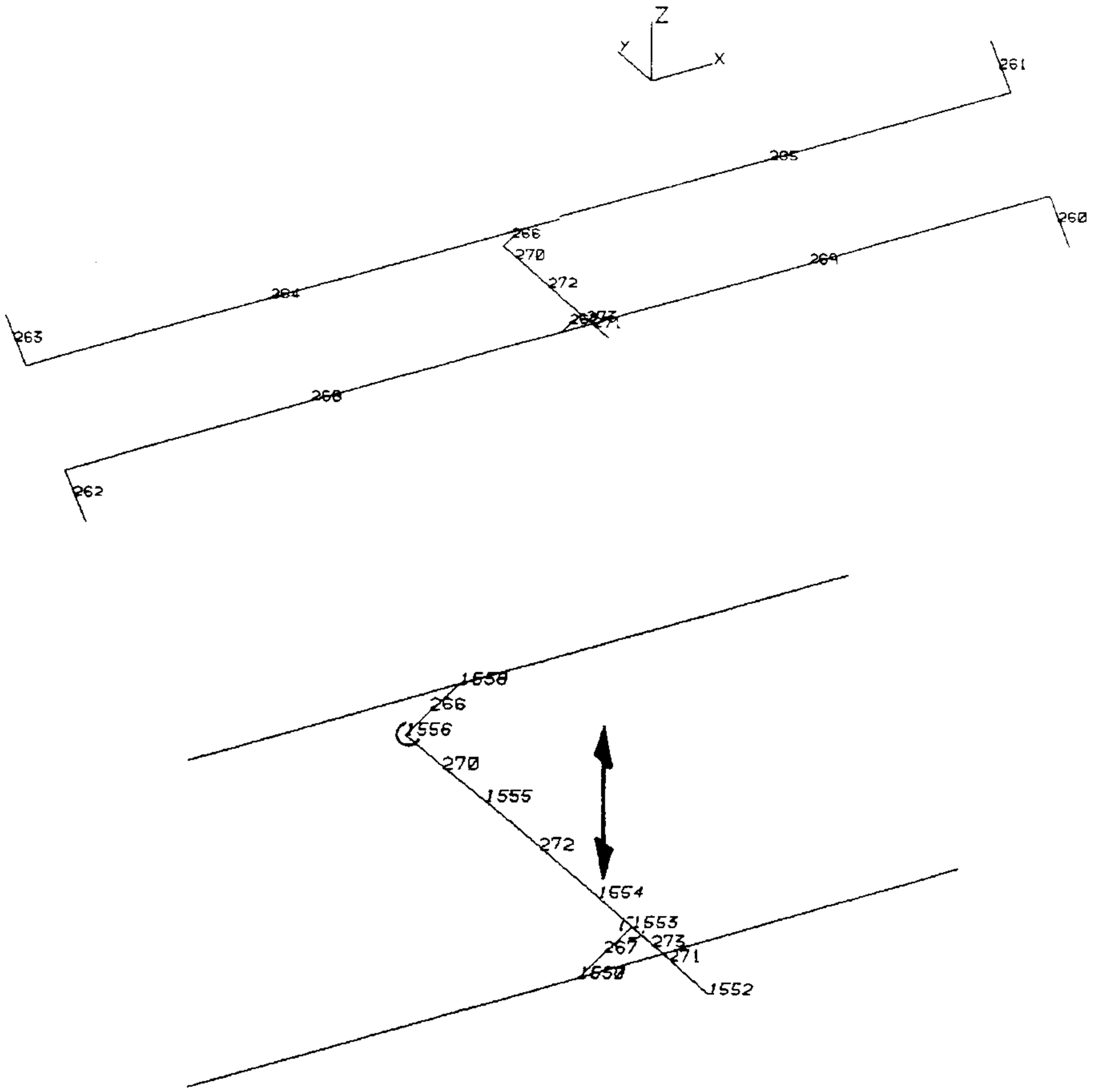

FIGURE 16 - A quartering view of the beam system used to excite the altitude axis for frequency response analysis. Beams 260/262 have the inertia and stiffness properties of the drive box and tangent arm, 261/263 the linear equivalent inertia and stiffness properties of the drive shaft assembly. Beams 268/269 and 264/265 are rigid weightless whiffle trees. Beams 266/270 and 267/271 are levers which pivot about nodes 1556 and 1553, respectively. Whiffle tree beam 272/273, with the levers and other whiffle trees, cause the single excitation applied at node 1554 to distribute equally to the four drive points.

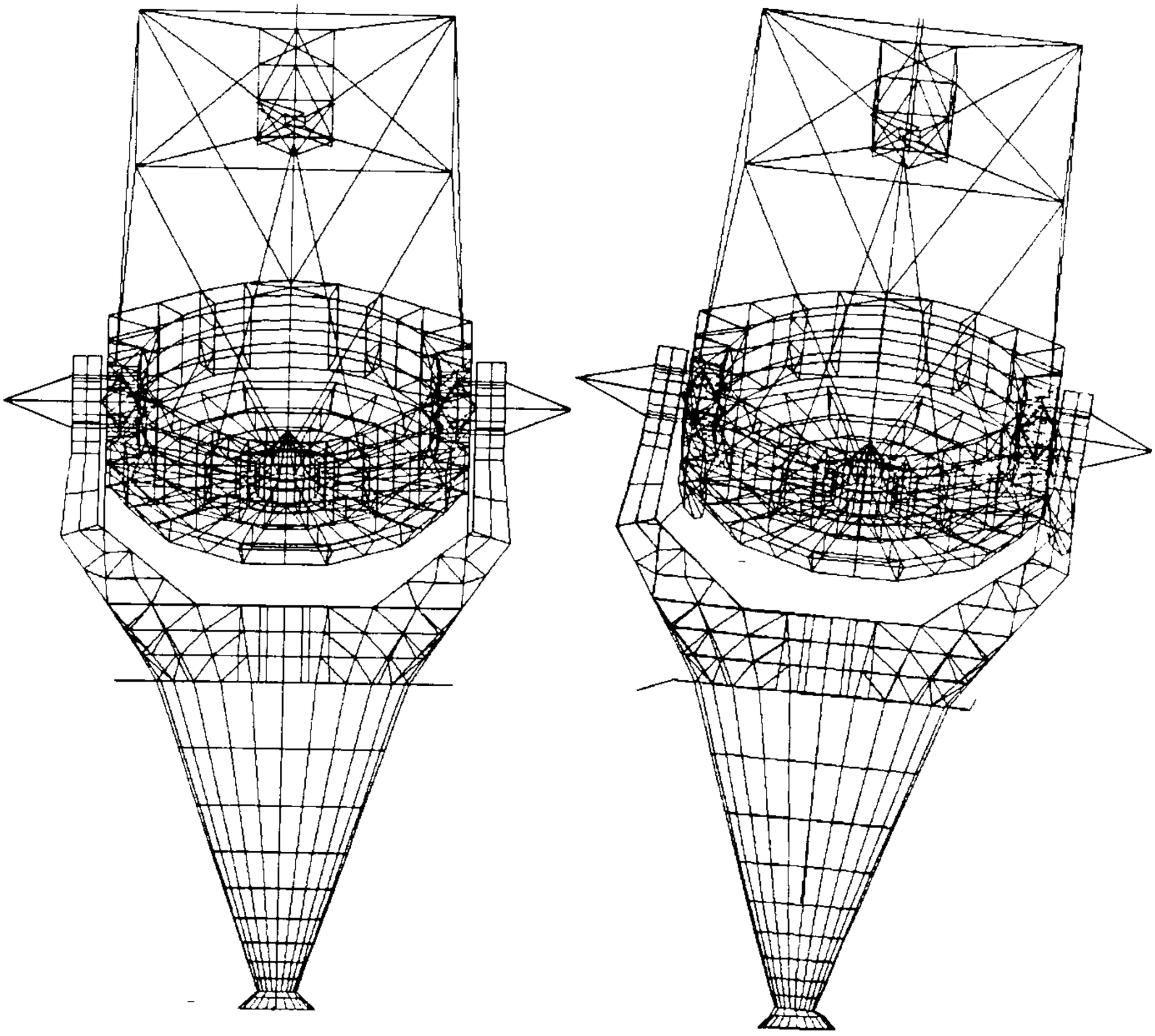

FIGURE 17 - Front view of the undisturbed telescope and modeshape 1, lateral translation, at 8.2 hz. Fork optimizing was performed in earlier work, OSS and upper azimuth support system optimizing during the recent analysis, raising this frequency from 7.6 hz in the June 1990 report. While this mode was found to not couple to the drives on either axis, there is some pointing error and optical misalignment. Since the drives can neither excite nor damp this modeshape, it is important that its frequency be as high as possible.

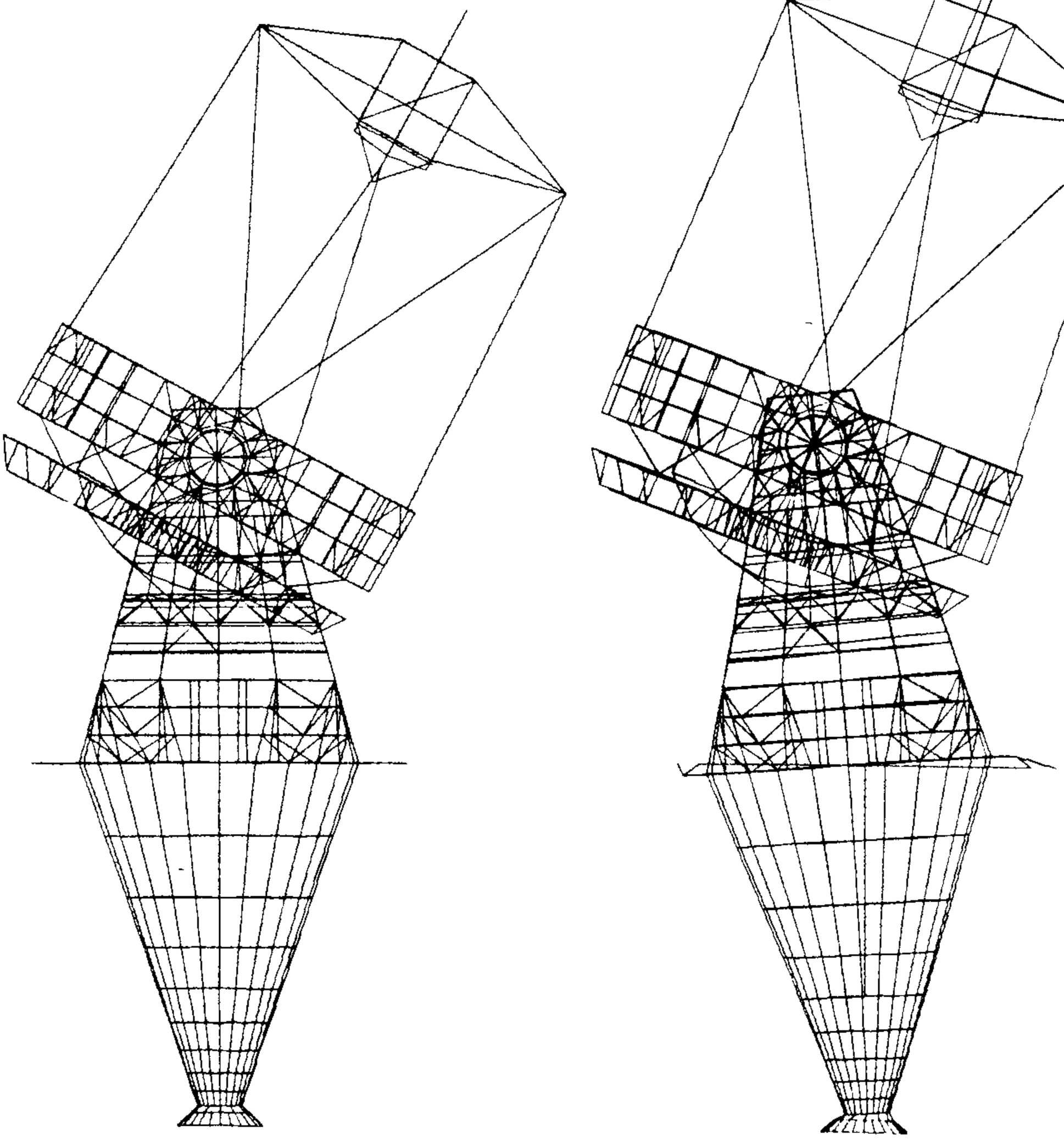

FIGURE 18 - Side view of model WIYNTM60, the conventionally-constrained modal analysis model. The left view is of the undisturbed model with the OSS 30° from zenith. The right view is of modeshape 2, fore-aft translation, at 8.8 hz. While this is fundamentally the same (lowest) mode which couples to the altitude drives, it does so at a slightly higher frequency without the inclusion of the "locked encoder", or infinitely stiff drives used here. This mode in the frequency response analysis was therefore 9.4 hz. (see Figure 21 below). Note that the rotation of the OSS (about an axis parallel to the altitude axis) is in phase with the fork rotation, as compared to modeshape 6 (Figure 19), where they are out of phase.

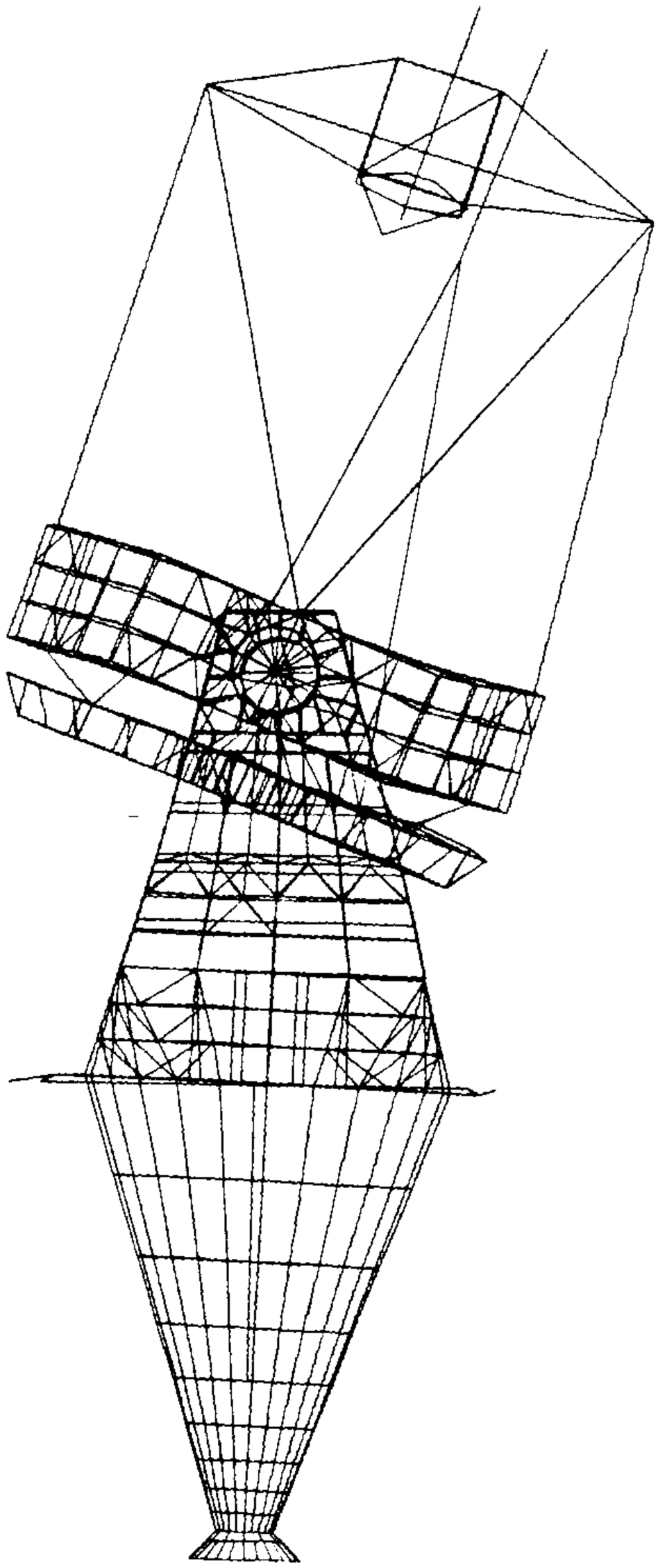

FIGURE 19 - Mode no. 6, "locked encoder altitude", at 17.3 hz. Note that the OSS rotation is out of phase with the fork rotation as compared to Figure 18, fore-aft translation. While conventional thought has been that this modeshape drives control system performance, the frequency response analysis shows that it does not. In fact, the second resonance in the magnitude and phase response plots[2] doesn't occur until the vertical translation mode, at 25.4 hz. (Figure 22).

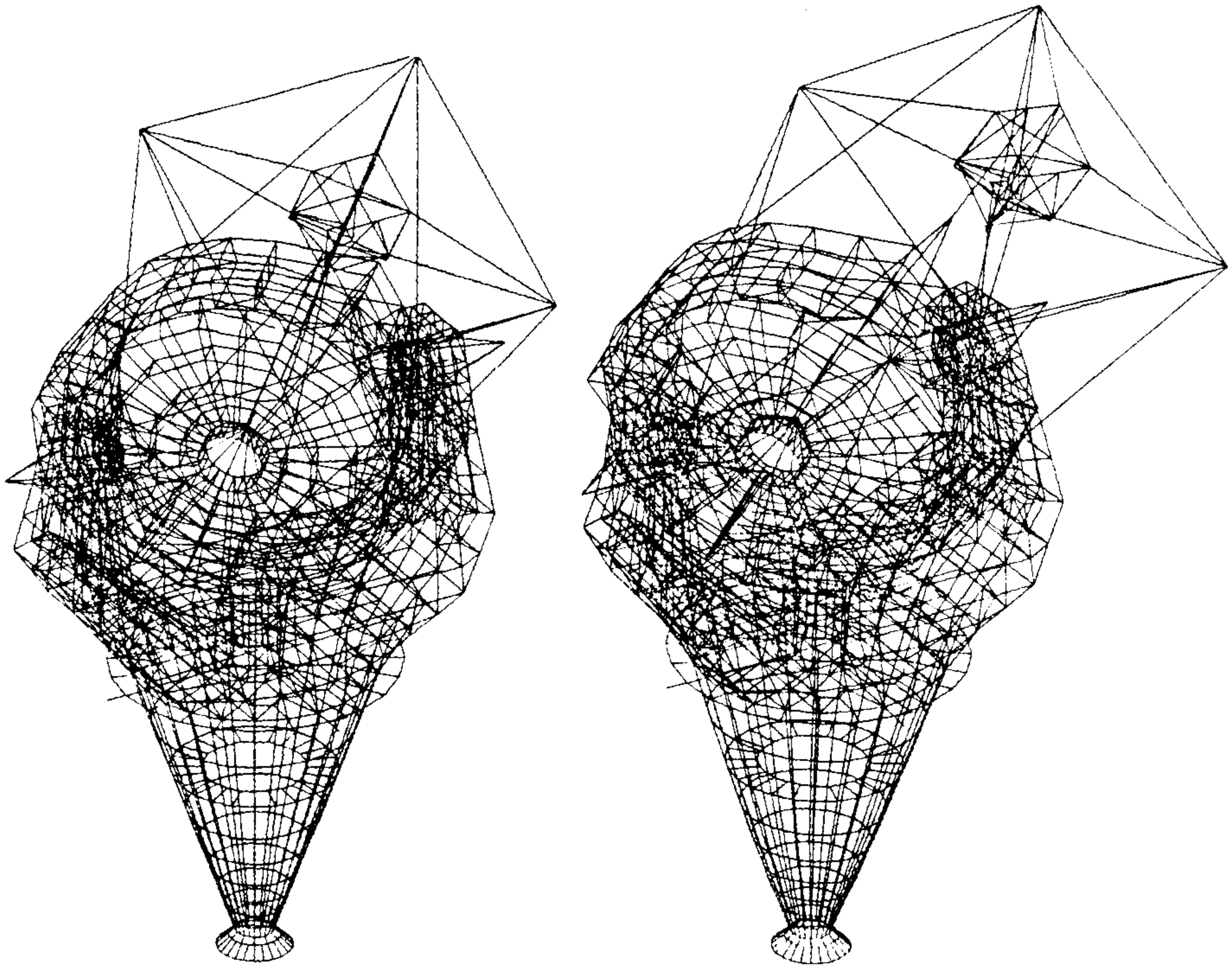

FIGURE 20 - Quartering view of the system undisturbed (left view) and of the fourth primary modeshape, locked encoder rotation about the azimuth axis, at 22.4 hz. While it has generally been thought that this mode is the critical one in terms of control system effects, it is not. (See the frequency response analysis discussion in the body of this report).

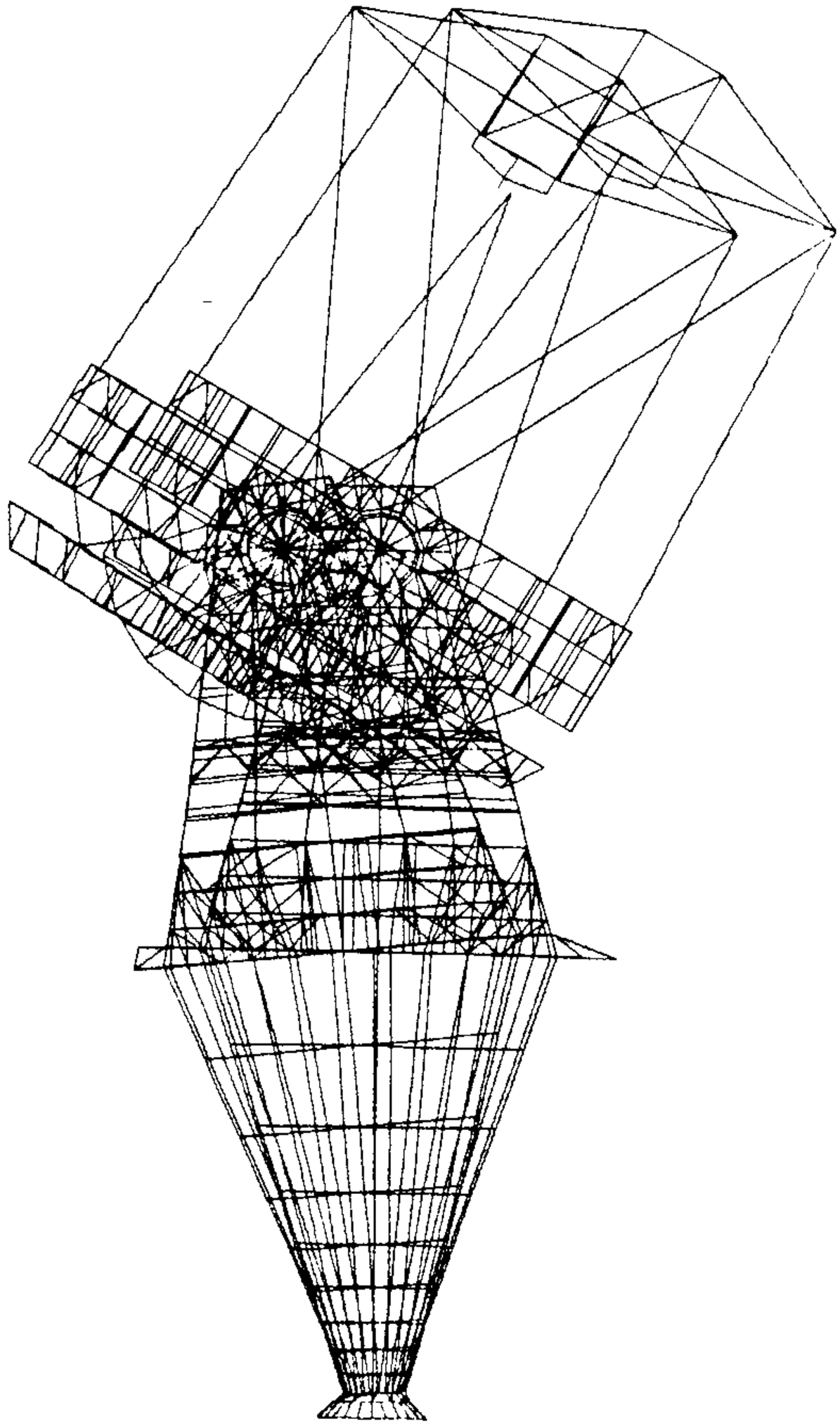

FIGURE 21 - Side views undisturbed and of the first altitude frequency response resonance (model WIYNTM35), fore-aft translation with a frequency of 9.4 hz.

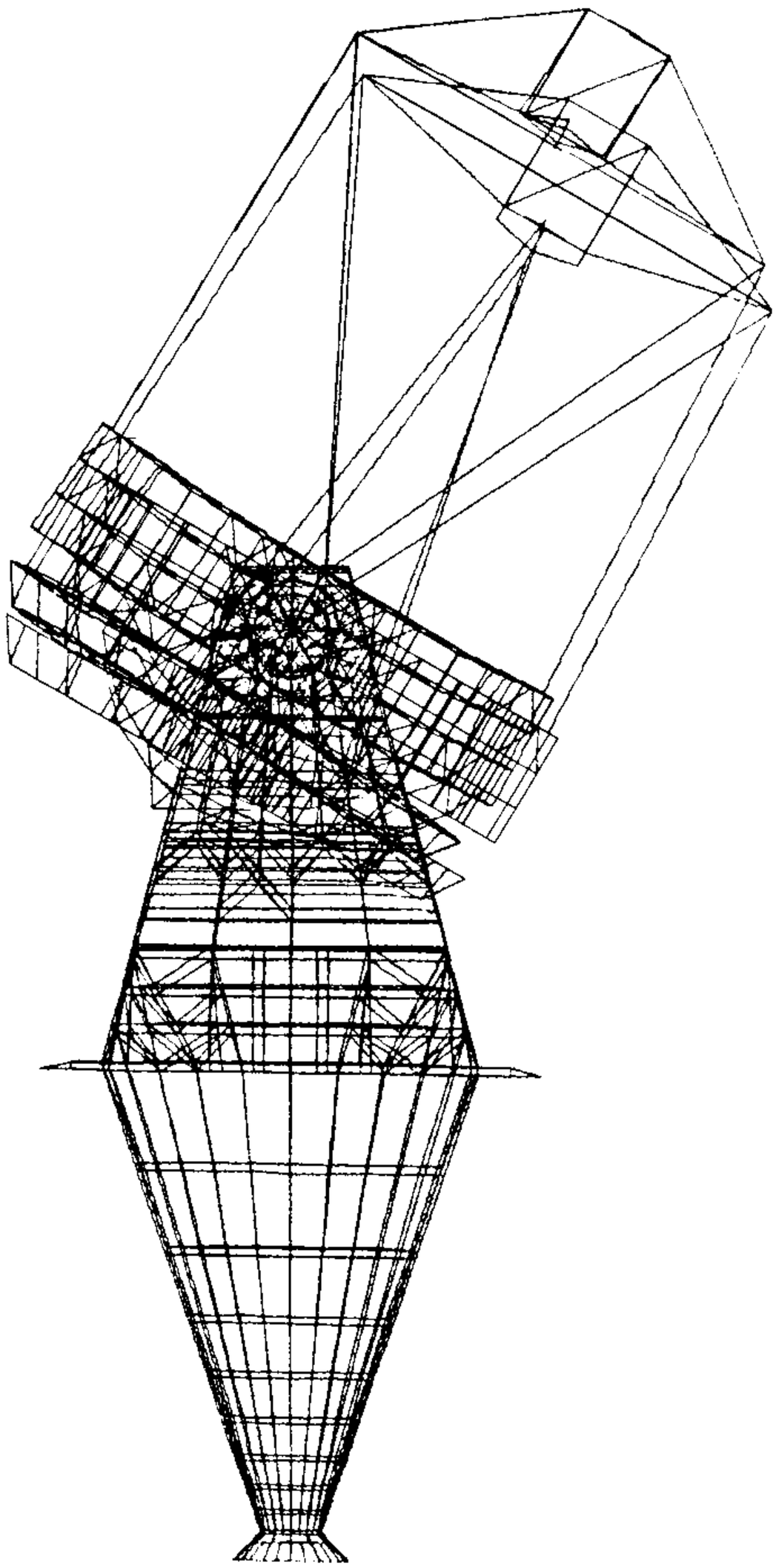

FIGURE 22 - Side views undisturbed and of the second altitude frequency response resonance (model WIYNTM35), vertical translation with a frequency of 25.4 hz.

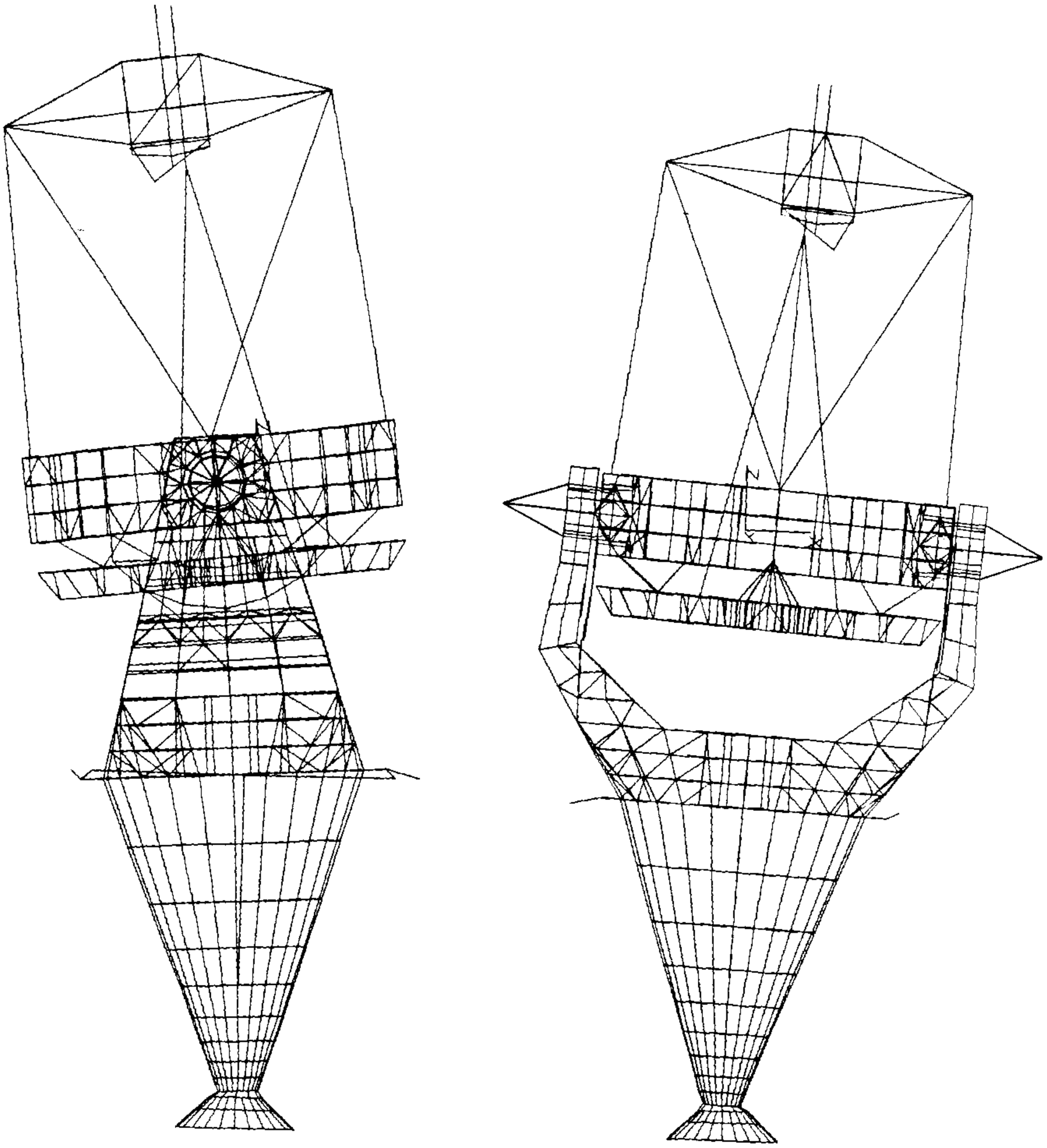

FIGURE 23 - Model WIYNTZ58 - the complete telescope, zenith pointing, under wind load. Applied wind load was 15 mph *acting upon the telescope structure.* This is equivalent to an approximate 45 mph ambient wind remote from the enclosure. Left view is a side view under front wind, with deflections scaled 60,000:1. Right view is a front view under side wind, also scaled 60,000:1. Note that the baffle deflection is not meaningful, since it was included just as a convenient means of applying nodal loads.

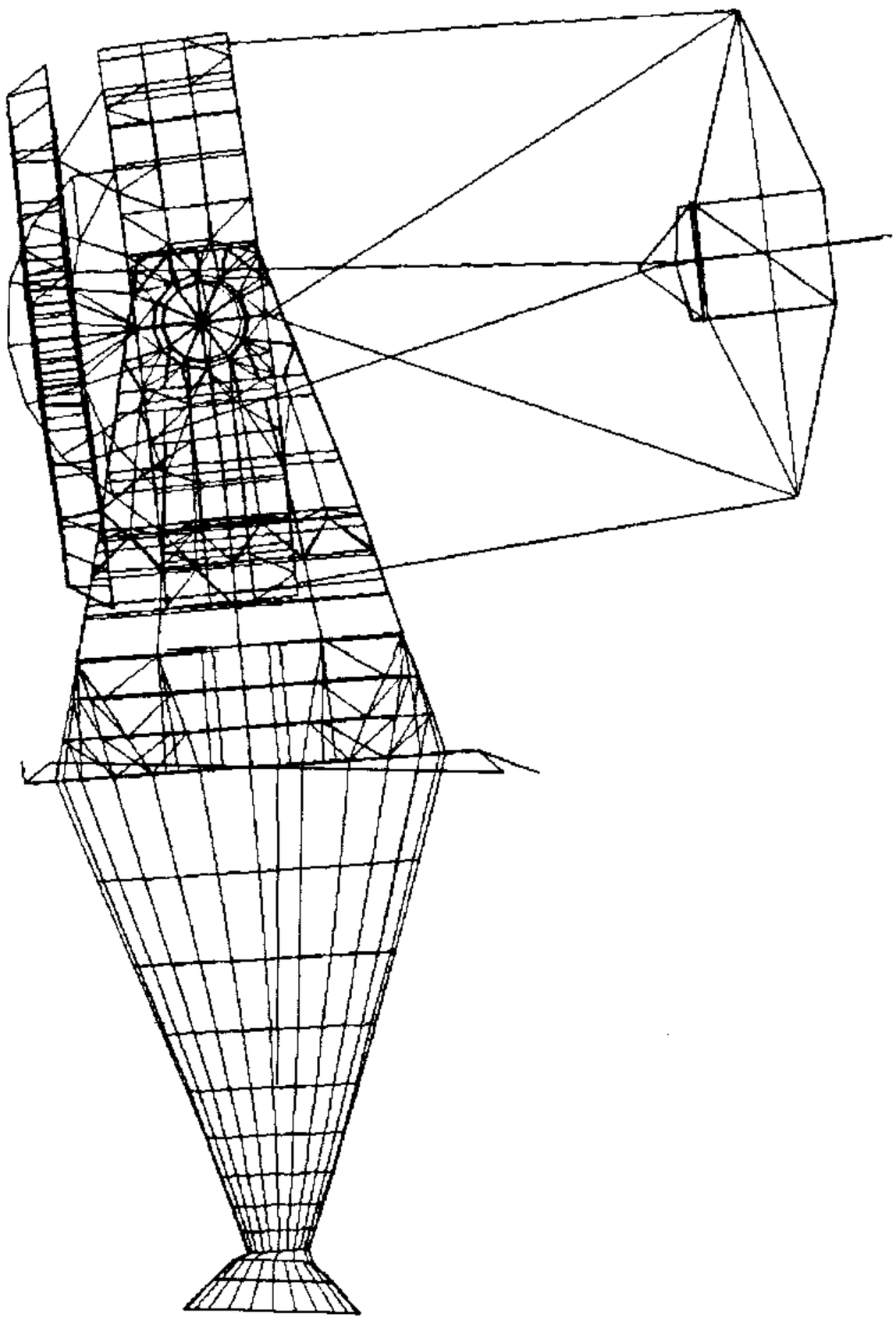

FIGURE 24 - Model WIYNTH59 - the complete telescope, horizon pointing. This side view shows the deflected shape of the system under front wind, scaled 100,000:1.

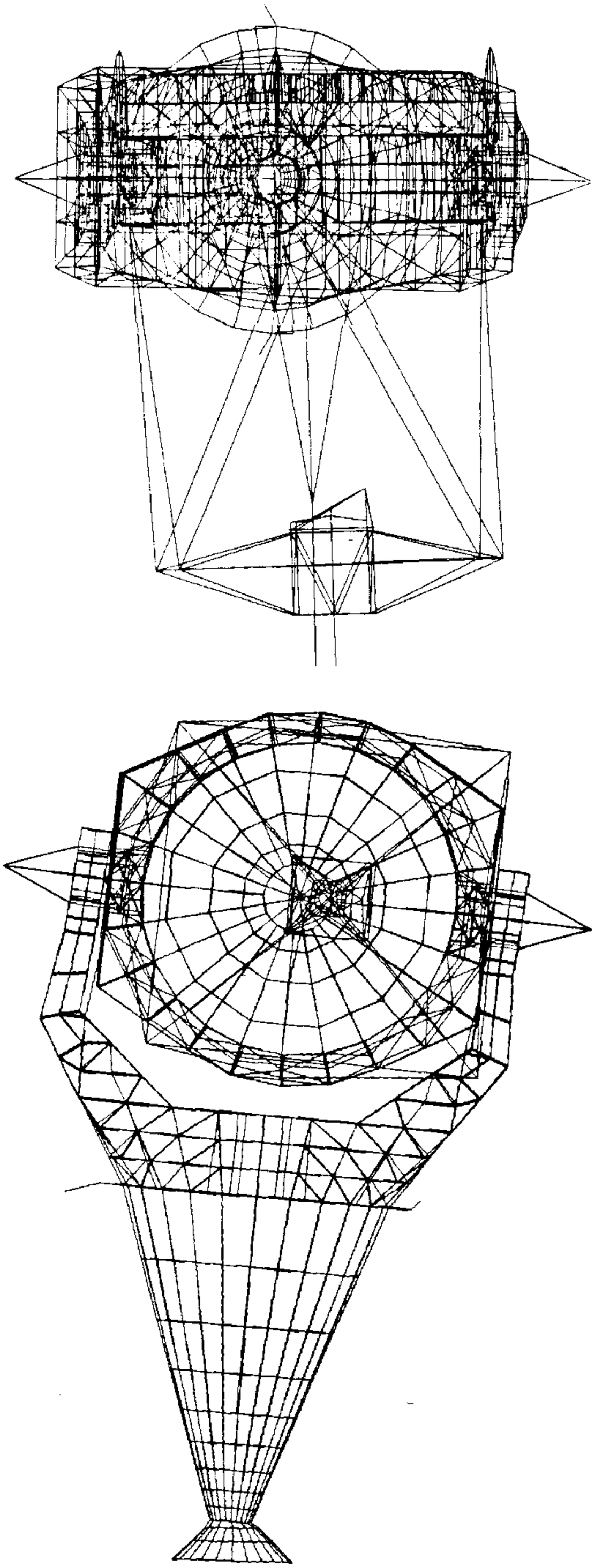

FIGURE 25 - Model WIYNTH59 top and front views under horizon side wind. Deflections are scaled 100,000:1.

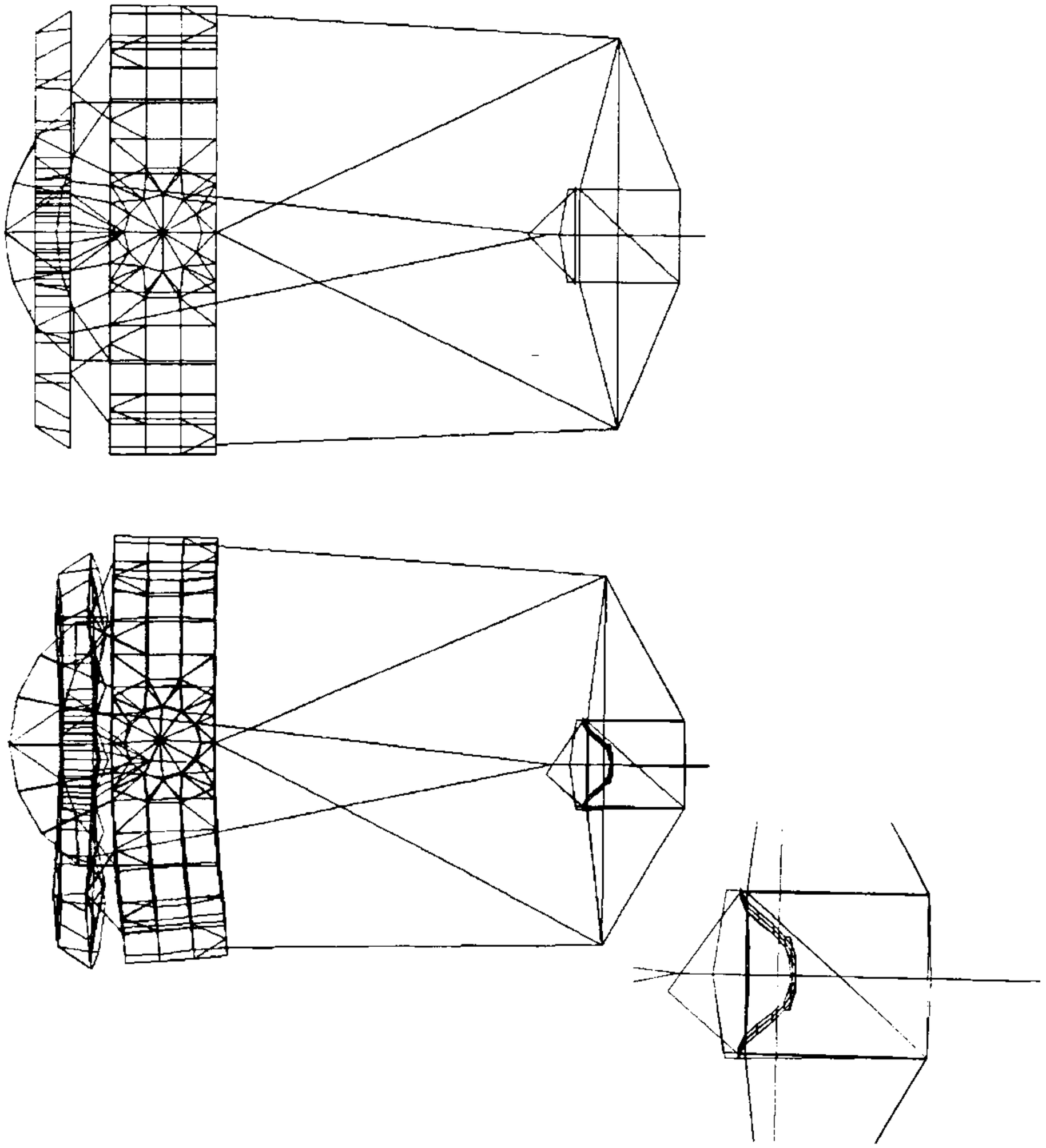

FIGURE 26 - Side view of model OSS57, load case 3; negative zenith gravity plus positive horizon gravity. If the optics are perfectly aligned at zenith, this would be the deflected shape of the OSS after rotating through the gravity field, scaled 1,000:1. Note that secondary and primary are virtually perfectly aligned due to optimization of both the primary and secondary end truss members. The primary mirror cell is rotating down toward the secondary due to the primary truss geometry.

APPENDIX

MAGELLAN PROJECT 8 METER TELESCOPE

FREQUENCY RESPONSE BY FINITE ELEMENT ANALYSIS

In Report No. 29, frequency response equations for a highly simplified telescope model were derived. The magnitude response was plotted (output base position per unit of applied peak torque) against excitation frequencies, under steady-state forced vibrations. The phase response (base output as compared to torque input) was also plotted against the same excitation frequencies.

The same magnitude and phase responses have been predicted using the finite element method. This two-step process involves determining natural frequencies and modeshapes (modal analysis) followed by a separate frequency response analysis. Thirty-nine excitation frequencies were applied (spaced approximately logarithmically) from 0.955 hz. to 1 khz. The simplified finite element model is shown in the attached graphics plots. An abbreviated frequency response output file is also included.

As shown on the attached magnitude and phase response plots, the analytical and finite element methods are in excellent agreement. As explained with the magnitude response plot, the low-frequency variation between the two methods results from the finite element approach not being able to accommodate rigid body modes. However, it can be concluded that the two methods are in excellent agreement above about 4 hz., allowing proper identification of all real resonances and antiresonances.

The finite element approach can therefore now be applied to the much more complex condition of the real telescope model, which includes very detailed distribution of mass and stiffness.

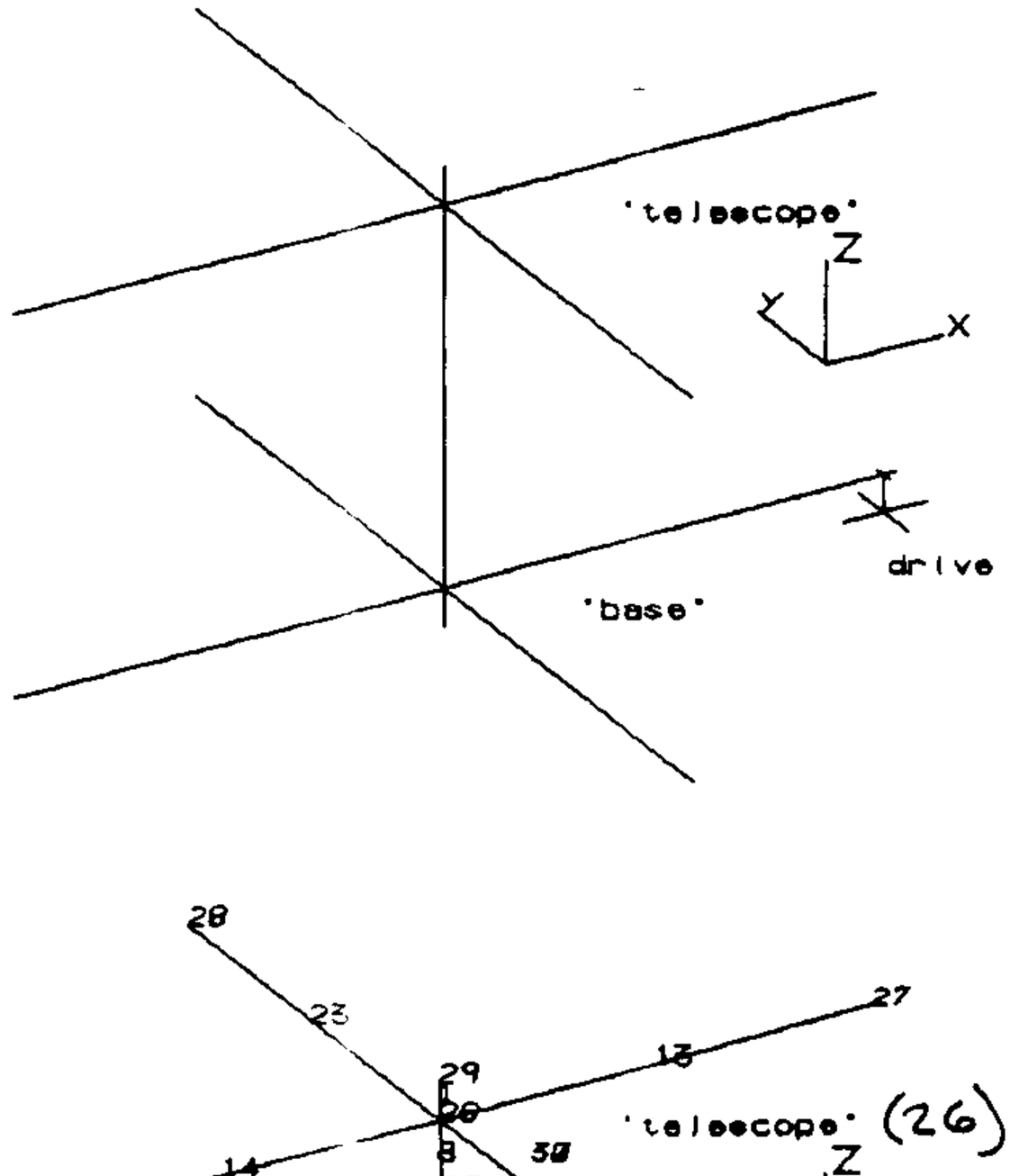
'telescope'
Z
Y
X
drive
'base'
28
23
29
27
13
20
14
26
8
30
23
24
9
24
22
10
19
21
11
21
20
12
26
22
'telescope' (26)
'base' (10)
drive

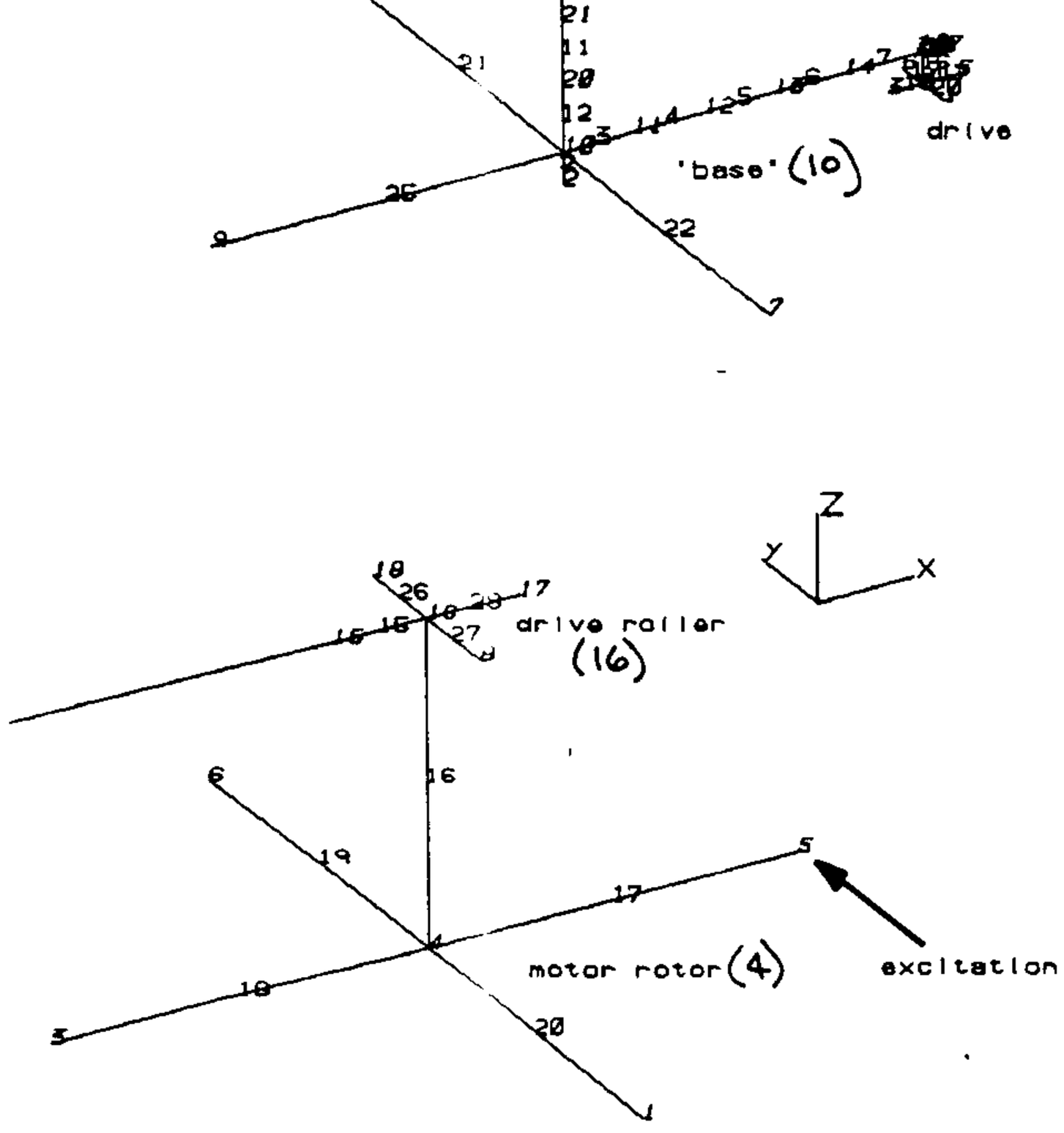
Z
Y
X
18
26
17
16
15
27
drive roller
(16)
6
16
19
5
17
motor rotor (4)
excitation
10
3
20
1

MAGELLAN PROJECT 8 METER TELESCOPE

MAGNITUDE RESPONSE - ANALYTICAL vs. FEA RESULTS, REPORT. No. 29

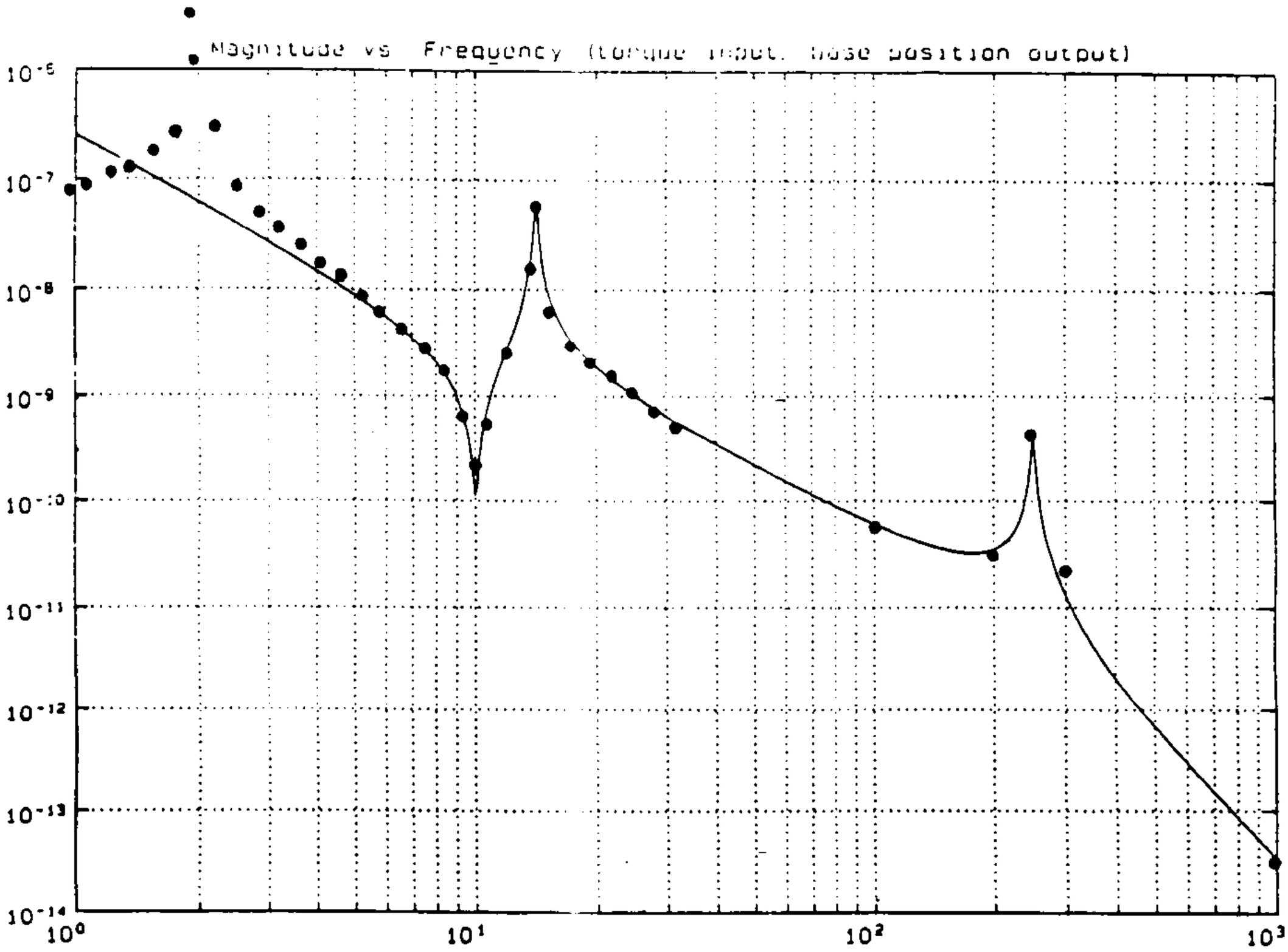

The magnitude response of the model system predicted analytically (ref. Report No. 29). Note the one antiresonance followed by two resonances. This response was calculated using the model parameters given in the report with a small amount of damping (0.01 damping ratio) added to keep the peaks and valley finite

The magnitude response of the model system predicted by finite element analysis. The "free boundary" condition was simulated by the use of soft support springs connecting the model to ground. Softer springs yielded premature program termination due to "rigid body modes". The first resonance (1.938 hz.) is therefore the unreal "nearly rigid body mode" caused by these springs. Beyond this effect correlation between the analytical and FEA results is excellent.

MAGELLAN PROJECT 8 METER TELESCOPE

PHASE RESPONSE - ANALYTICAL vs. FEA RESULTS, REPORT No. 29

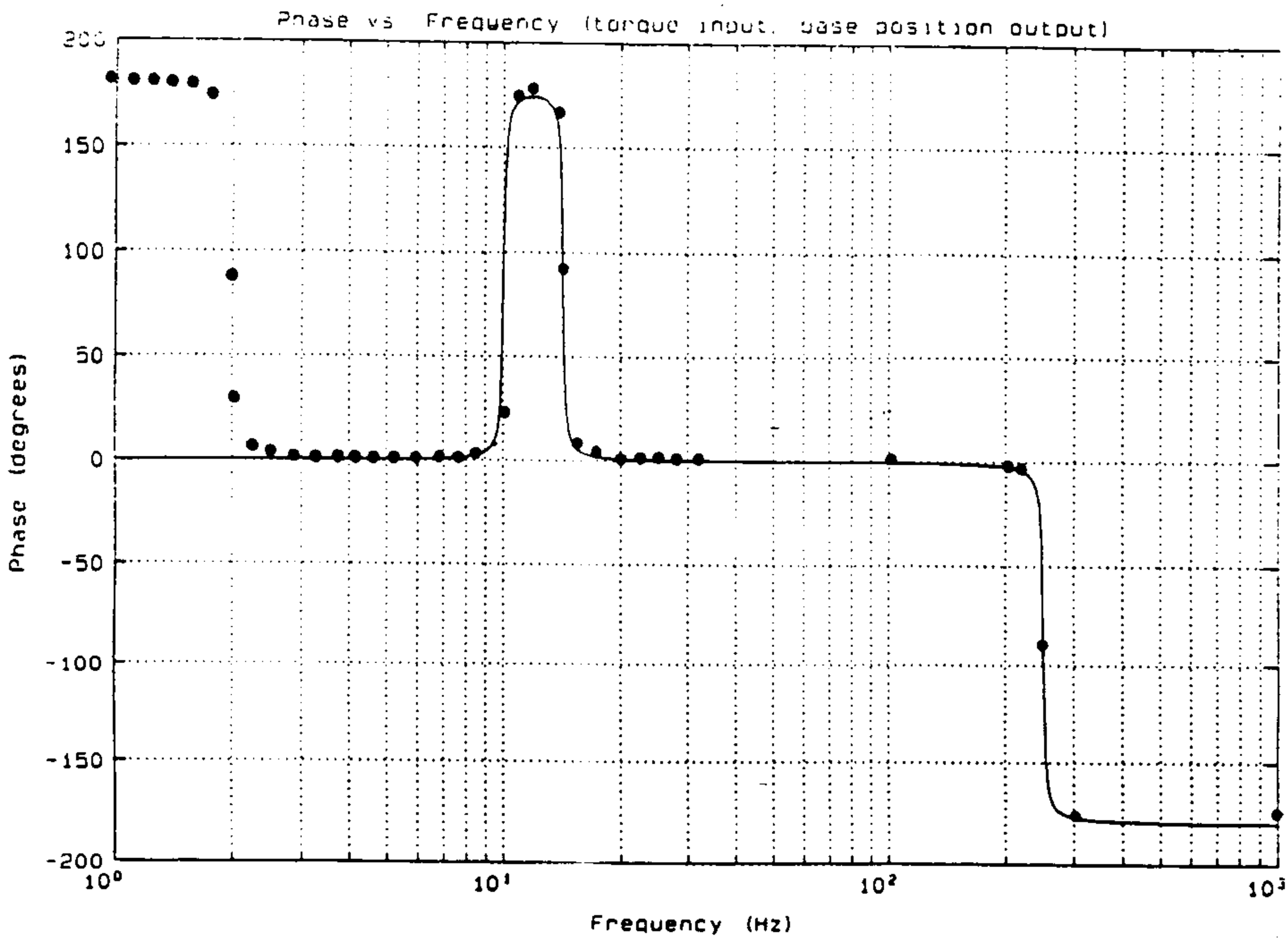

The phase response of the model system predicted analytically (ref. Report No. 29). Note the small area of phase lead followed by a steep transition to negative phase angles. This response was calculated using the model parameters given in the text with a small amount of damping added. This plot has been shifted 180 degrees to remove the effect of the rigid body mode and center the plot around 0 degrees.

• • • • The phase response of the model system predicted by finite element analysis. The "nearly rigid body mode" causes an artificial phase variation below 1.938 hz. (ref. magnitude response plot). The finite element analysis program used employs a SRSS (square root sum of squares) calculation and therefore all output phases angles are positive. Phase sign has been plotted here using the phase signs from the analytical method.

WIYN AZIMUTH AXIS MAGNITUDE AND PHASE RESPONSES

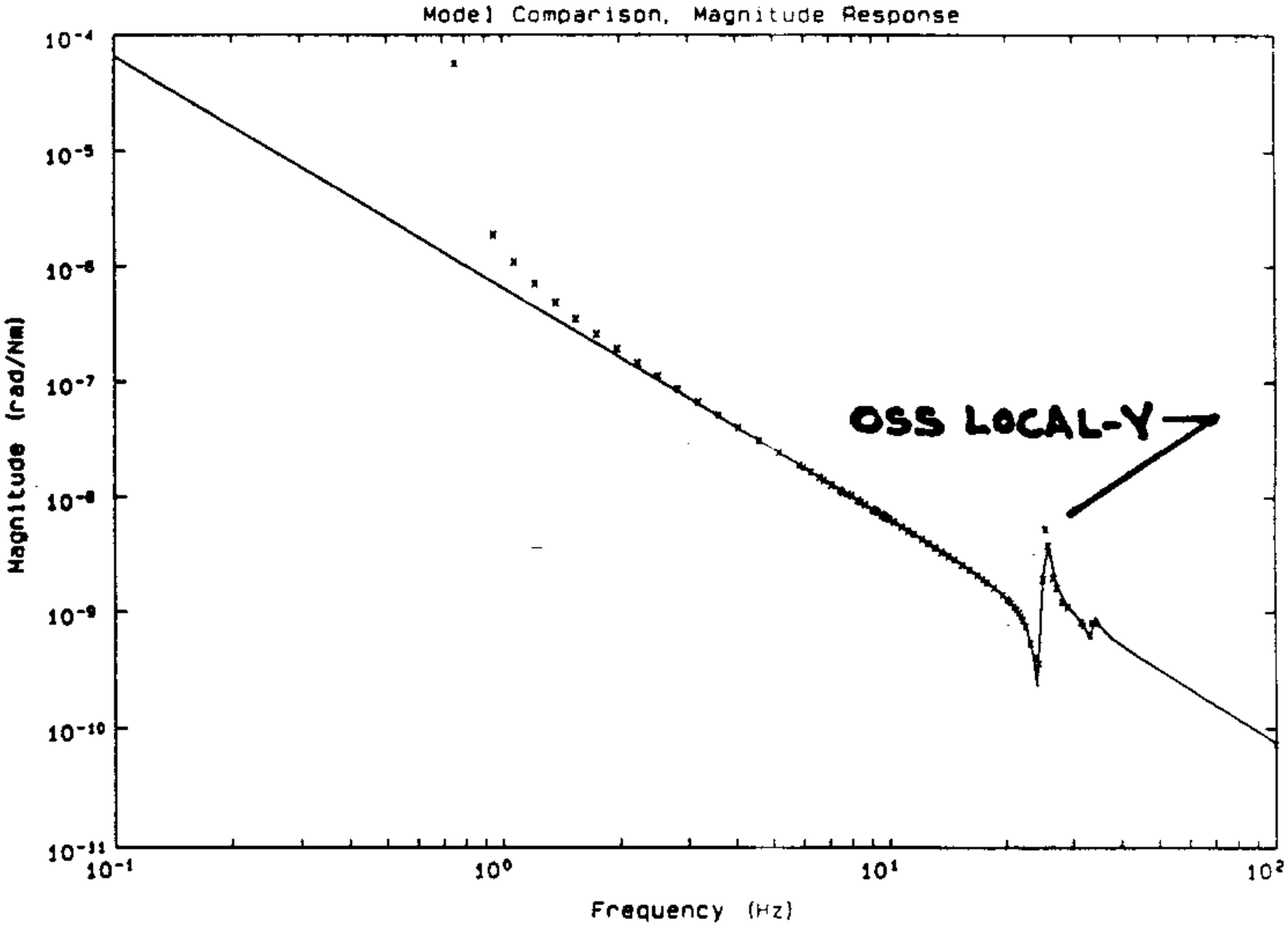

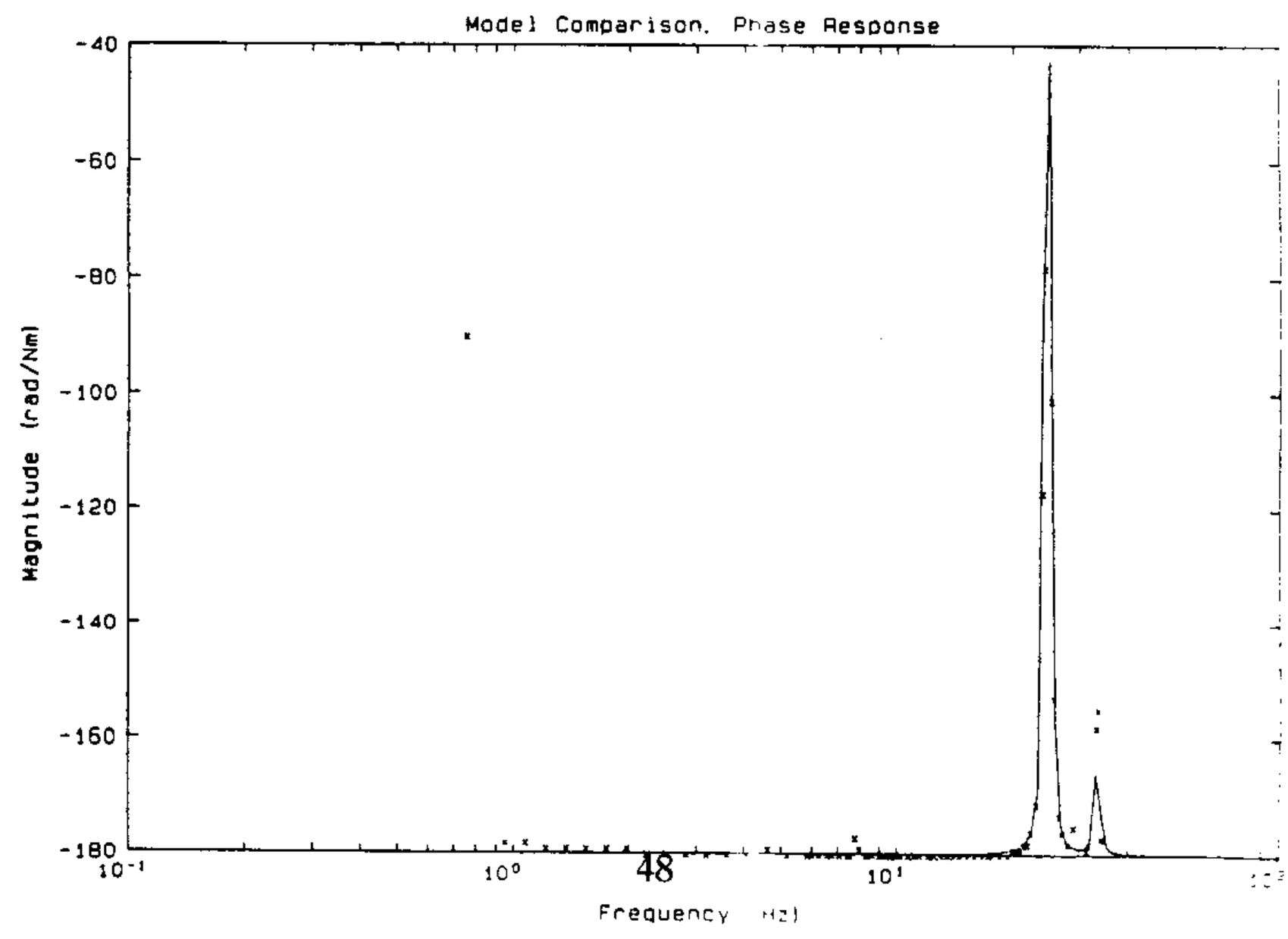

WIYN ALTITUDE AXIS MAGNITUDE AND PHASE RESPONSES

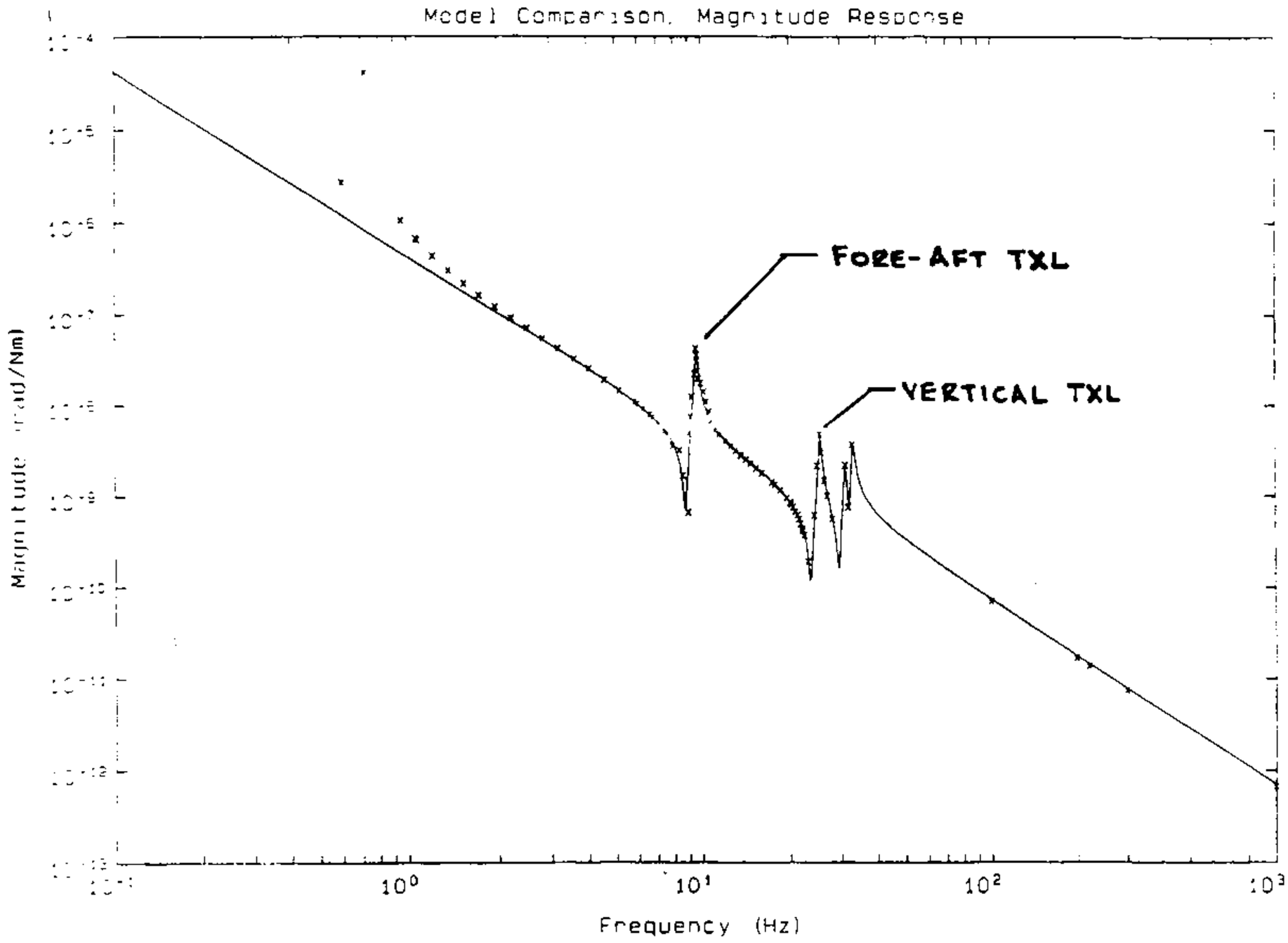

ABSOLUTE ZENITH WIND DISPLACEMENTS

```
1**** Algor (c) Linear Stress Analysis  SSAPOH  Rel. 02/25/91, Ver. 9.20/387

      DATE: MAY 30,1991
      TIME: 10:35 AM
      INPUT FILE.............WIYNTZ58
-----------------------------------------------

      ZENITH WIND MODEL;WIYNTM32 FORK + OSS57

1**** CONTROL INFORMATION

      number of node points          (NUMNP)   =          1682
      number of element types        (NELTYP)  =             2
      number of load cases           (LL)      =             2


1**** STATIC ANALYSIS

      LOAD CASE =  1 = ZENITH FRONT WIND

      Displacements(inches)/Rotations(degrees) of unrestrained nodes

  NODE          X-            Y-            Z-            X-            Y-            Z-
 number   translation translation translation    rotation      rotation      rotation

PMT 1649   1.3420E-07  6.0413E-04  1.0181E-05 -1.1910E-04  1.5769E-08 -4.4295E-08
SMT 1650   6.8415E-07  7.0792E-04  9.8849E-06 -1.3225E-04 -1.6714E-06  1.5885E-07


1**** STATIC ANALYSIS

      LOAD CASE =  2 = ZENITH SIDE WIND

      Displacements/Rotations(degrees) of unrestrained nodes

  NODE          X-            Y-            Z-            X-            Y-            Z-
 number   translation translation translation    rotation      rotation      rotation

PMT 1649   3.8908E-04  1.3306E-06  2.3000E-06 -5.6615E-07  5.3371E-05  8.1124E-07
SMT 1650   4.7955E-04  2.6949E-06  2.5964E-06  1.2575E-06  5.9695E-05  8.5746E-07


NODE 1649 - PRIMARY MIRROR TARGET (PMT)
NODE 1650 - SECONDARY MIRROR TARGET (SMT)


1**** TEMPORARY FILE STORAGE (MEGABYTES)
      ---------------------------------
       TOTAL       :  41.111

1**** End of file
```

ABSOLUTE HORIZON WIND DISPLACEMENTS

```
1**** Algor (c) Linear Stress Analysis  SSAPOH  Rel. 02/25/91, Ver. 9.20/387

      DATE: MAY 31,1991
      TIME: 08:40 AM
      INPUT FILE.............WIYNTH59
-----------------------------------------------

HORIZON WIND; WIYNTZ58 FORK BUT X AND Z ROTNS OF NODES 704-706 RESTRAINED
AND OSS57 BUT 2" DIA. PMT, TO REDUCE MAX/MIN RATIO BELOW 1E10 WARNING LEVEL
(RESULTS ARE THE SAME AS EARLIER MODEL WITH MAX/MIN WARNING)


1**** STATIC ANALYSIS

      LOAD CASE = 1 - HORIZON FRONT WIND

      Displacements/Rotations(degrees) of unrestrained nodes

  NODE          X-          Y-          Z-          X-          Y-          Z-
 number translation translation translation    rotation    rotation    rotation

PMT 1649-1.8344E-09  3.1696E-04  2.3109E-04 -8.8959E-05  2.7667E-08 -3.8359E-08
SMT 1650-2.9330E-06  3.4550E-04  2.1820E-04 -1.0069E-04 -9.6554E-06  1.3583E-05


1**** STATIC ANALYSIS

      LOAD CASE = 2 - HORIZON SIDE WIND

      Displacements/Rotations(degrees) of unrestrained nodes

  NODE          X-          Y-          Z-          X-          Y-          Z-
 number translation translation translation    rotation    rotation    rotation

PMT 1649 2.5332E-04  9.8139E-07  4.0070E-06 -3.9278E-07  4.0116E-05  1.5434E-05
SMT 1650 3.3937E-04  8.4203E-07  5.2467E-06  9.1412E-07  3.9829E-05  2.1027E-05


NODE 1649 - PRIMARY MIRROR TARGET
NODE 1650 - SECONDARY MIRROR TARGET

40.357 MEGABYTES TOTAL TEMPORARY FILE STORAGE
94.471 MINUTES TOTAL PROCESSING TIME INCLUDING STRESS OUTPUT

1**** End of file
```

ABSOLUTE GRAVITY DISPLACEMENTS

**** DISPLACEMENT POST-PROCESSING OF OSS57.DO

LOAD CASE 3 SCALE FACTOR 1.000E+00

ZENITH GRAVITY REMOVED, HORIZON GRAVITY APPLIED

NODE	GLOBAL X TRANSLATION INCHES	GLOBAL Y TRANSLATION INCHES	GLOBAL Z TRANSLATION INCHES	GLOBAL X ROTATION (DEGREE)	GLOBAL Y ROTATION (DEGREE)	GLOBAL Z ROTATION (DEGREE)
TMT 327	-1.5190E-06	-9.1639E-03	1.0523E-02	9.4539E-04	-2.7541E-05	-1.2364E-05
PMT 576	8.7086E-05	-9.6268E-03	1.0077E-02	3.5507E-04	2.2468E-05	-1.2107E-05
SMT 577	2.2660E-04	-9.6480E-03	1.2747E-02	3.5392E-04	-8.8271E-04	-1.7673E-03

NOTE - NODE 327 = TERTIARY MIRROR TARGET (TMT)
NODE 576 = PRIMARY MIRROR TARGET (PMT)
NODE 577 = SECONDARY MIRROR TARGET (SMT)

**** MAGNITUDE MAXIMA

NODE	GLOBAL X TRANSLATION	GLOBAL Y TRANSLATION	GLOBAL Z TRANSLATION	GLOBAL X ROTATION (DEGREE)	GLOBAL Y ROTATION (DEGREE)	GLOBAL Z ROTATION (DEGREE)
NODE	90	587	679	626	630	252
	3.2248E-03	-1.3549E-02	2.4208E-02	3.4594E-02	-3.4550E-02	1.7275E-02
NODE	259	580	666	705	701	98
	-3.1359E-03	-1.0256E-02	2.4203E-02	-3.4519E-02	3.4481E-02	-1.6838E-02
NODE	121	712	665	627	700	194
	-2.9876E-03	-1.0096E-02	2.4194E-02	3.4328E-02	-3.4341E-02	1.2192E-02
NODE	232	713	678	704	631	23
	2.9437E-03	-1.0014E-02	2.4193E-02	-3.4154E-02	3.4187E-02	-1.2145E-02
NODE	257	583	677	628	628	26
	-2.7556E-03	-9.8611E-03	2.4193E-02	3.3820E-02	-3.3772E-02	-1.1818E-02
NODE	92	586	670	703	703	191
	2.6872E-03	-9.8414E-03	2.4190E-02	-3.3748E-02	3.3724E-02	1.1729E-02
NODE	108	608	652	636	632	84
	2.2954E-03	-9.8260E-03	2.4188E-02	3.3699E-02	-3.3632E-02	-1.1402E-02
NODE	317	584	662	629	702	238
	1.9833E-03	-9.7111E-03	2.4185E-02	3.3565E-02	-3.3583E-02	1.1303E-02
NODE	104	578	669	630	699	116
	1.9700E-03	-9.6781E-03	2.4185E-02	3.3559E-02	3.3552E-02	-1.1182E-02